Performance Analysis and Optimization of Solar Thermochemical Reactor By Diluting Catalyst with Encapsulated Phase Change Material

Zhao Ma[a], Ming-Jia Li[a], Ya-Ling He[a,] *, K. Max Zhang[b]
a. Key Laboratory of Thermo-Fluid Science and Engineering of MOE, School of Energy and Power Engineering, Xi'an Jiaotong University, Xi'an, Shaanxi 710049, China
b. Sibley School of Mechanical and Aerospace Engineering, Cornell University, Ithaca, NY 14853, USA
*Corresponding author. Tel/Fax: +86-29-82665930
Email Address: yalinghe@mail.xjtu.edu.cn & hylxjtu@gmail.com

Abstract: Solar thermochemical reactor, which can produce solar fuel at low cost, suffers discontinuous low-efficiency performance due to solar radiation fluctuation caused by cloud passage. To achieve highly efficient steady and dynamic performance of solar chemical reactor with less catalyst, in this study, catalytic activity is adjusted by diluting catalyst with encapsulated phase change material. At first, two-dimensional model of solar parabolic trough receiver reactors diluted with encapsulated phase change material is established and validated. Then, effect of catalytic activity on performance of reactor is discussed. Afterwards, one-dimensional model is derived from two-dimensional model to train Back Propagation neural network for quick and precise performance prediction of reactor. Finally, optimal catalytic distribution is obtained by genetic algorithm and Back Propagation neural network, and steady and unsteady performance of reactor between uniform and optimal catalytic distribution are compared. The results show that when catalytic activity decreases from 1.0 to 0.2, steady methanol conversion efficiency and production rate of H_2 are reduced by 8.4 % and 9.9 %, and reactor shows more stability under unsteady condition of solar radiation. One-dimensional model derived in present study is accurate enough and time-saving compared to two-dimensional model. And compared to reactor fully packed with catalyst, reactor with optimal catalytic distribution can achieve similar steady performance with 56 % less of catalyst, but shows better stability under the fluctuation of solar radiation.

Keywords: Solar thermochemical reactor; Solar radiation fluctuation; Phase change material; Catalytic activity's distribution; One-dimensional model

1. Introduction

Solar energy has increasingly been considered as a promising resource to energy crisis and global environmental problem[1]. Solar thermochemical reaction which can produce solar fuel, such as hydrogen or syngas, has attracted lots of attention due to its high efficiency, low cost and no pollution[2]. In solar thermochemical reaction, solar energy is concentrated to provide heat for chemical reactor and stored in solar fuels which can be further converted to electricity by fuel cell, gas turbine or internal combustion engine[3]. According to the operational temperature of chemical process, solar thermochemical reactions can be roughly sorted into two groups[4]: high temperature process and middle-and-low temperature process

Usually, high temperature solar thermochemical reactions operates above 800 ℃[4], such as H_2O and CO_2 splitting[5], methane reforming[6] and biomass gasification[7]. Chuayboonab and Abanades et al. [6] experimentally investigated the solar-driven methane and H_2O/CO_2 splitting in the temperature range of 950-1050 ℃ and the ceria cycling stability was also examined. They found that the highest solar-to-fuel conversion efficiency can reach 5.22 %. High operation temperature may lead to the decrease of system's thermal efficiency due to heat loss and optical loss, and also raise the technical difficulties for the design, fabricating and operation of such high temperature system[8], especially in large-scale commercial applications. Different from the high temperature chemical process, middle-and-low solar thermochemical reactions are often operated within 150-500 ℃[9], which shows great potential for real applications. One of the promising middle-and-low thermochemical reactions for hydrogen is methanol steam reforming reactions because of its advantages that methanol can be producible from biomass, stays in liquid state for easy transportation and manipulation, and has high H/C ratio[10]. For example, Liu and Jin et al. [11] experimentally tested a 5-kW solar thermochemical reactor for methanol steam reforming heated between 150-300 ℃, and their experimental results showed that methanol conversion efficiency can be higher than 90%

and thermal-chemical conversion efficiency was in the range of 30-50 %, which is competitive with high-temperature solar thermochemical reactions.

However, weather transients cause a large challenge to the life span and safe operation of solar power plants[12]. Suffered by solar radiation variation caused by cloud transients, the solar thermochemical reactor may endure the large temperature fluctuation, which can reduce the chemical conversion efficiency [12], deactivation of catalyst [13] and even lead to the sudden shut down of system [14]. Strategies have been explored to alleviate the adverse effect of solar radiation fluctuation, which can be divided into two types: active controlling strategy and passive thermal management. In active controlling strategy, the heliostats[15], flow rate of reactants[16] or additional equipment, such as electric heater[12], are often regulated to maintain the continuous high-performance operation of solar chemical reactor. For example, Rowe and Weimer et al.[12] employed feedback and predictive linear models controllers to regulate the solar-electric reactor for the production of syngas at 925 ℃ through the gasification of carbon under the cloud transient. They concluded that the controlling accuracy of model predictive control is more precise than that of feedback control. Meanwhile, it should be noted that the controlling performance of active controlling strategy is highly affected by the accuracy of solar radiation forecast, which is hard to be predicted precisely[17]. Moreover, the temperature detector may not be distributed uniformly or small sufficiently to detect micro-size hot or cold spot[18]. Also, controlling robustness and accuracy are difficult to be guaranteed in the control process of solar chemical reactor[12].

Another efficient way to maintain the continuous performance of solar chemical reactor is passive thermal management with phase change material (PCM), which can absorb/release large amount of latent heat at constant temperature during the phase transition. So far, PCM has widely applied in the thermal management of battery system to avoid the sudden uprising of temperature [19] and heat storage for the continuous operation of solar power plant[20]. Huang and Cheng et al[21] applied form-stable composite PCM in the thermal management of Li-ion battery pack experimentally. Their experimental results showed the battery temperature drops by 18 °C at 10 C discharge rate with flexible form-stable composite PCM, and Li-ion battery can safely work for an extended time within the upper temperature limit. Meanwhile, there are few studies on the application of PCM in the

thermal management of solar thermochemical reactors. Pattison and Baldea et al. [22] confined PCM in layer between the plates of reactor for auto-thermal methane-steam reforming reactor to avoid the unpredictable temperature excursion and that structure showed excellent disturbance rejection performance with hierarchical control structure. To mitigate the adverse effects of solar radiation fluctuations, Hatamachi and Gokon et al. [23, 24] applied PCM in the tubular solar chemical reactor for CO_2 reforming of methane (operated over 700 ℃), and bulk PCM is packed into shell side to form "double-wall" reactor. In their experiments, Na_2CO_3 is employed as phase change material and their experimental results demonstrated that the proposed "double-wall" reactor can realize stable operation when insulation fluctuates caused by cloud passage. Furthermore, to improve the heat transfer rate[25] of PCM which is often limited by its low conductivity, in the study of Su et al. [26], instead of in bulk state, phase change material is encapsulated by silica, called encapsulated phase change material (EPCM), and is mixed with catalyst to quench the local hot spots induced by non-uniform packing of catalyst and abrupt change of reaction rate. Their results showed that the EPCM can quenching the local hot point at initial stage and prevent thermal runaway. O. Odunsi et al. [18, 27] investigated temperature stability of Fischer Tropsch reactor in which catalyst is diluted with EPCM ($Sn@SiO_2$) homogeneously. Their results showed that better selectivity of long chain hydrocarbons (C_{5+}) to CH_4 can be achieved by mixing EPCM with catalyst. On the other hand, some researchers [28] try to improve the steady performance of exothermic reactor by adjust catalytic activity distribution through diluting catalyst by solid inertia particles. Lee and Varma et al.[29, 30] confirmed that the overall conversion of chemical reactor can be improved with proper distribution of catalytic material through experiments. Nie and Witt et al. [30] optimized the graded reactor activity profile for exothermic reaction to balance the heat generation by reaction with heat removal capacity and potentially improve chemical performance. Their results showed that compared with uniform distribution of catalytic activity, the 2-part optimized activity profile can improve the production rate by 26 %. It also should be noted that poor optimized activity profile can lead to thermal runaway even with catalyst dilution[28].

The literature review above indicates EPCM can well prevent the thermal runaway of exothermic reactor in chemical plants. However, the solar chemical reactor, which is different from the

exothermic reactor, is heated by solar energy and faces the fluctuation of solar radiation cause by weather transients. The potential of mix catalyst with EPCM to alleviate the adverse effect of solar radiation fluctuation is rarely investigated. On the other hand, as concluded from above discussion, that non-uniform distribution of catalytic activity has potential to improve the steady performance (such as such as conversion efficiency and production selectivity) of thermochemical reactor. However, in most of these studies, catalyst is diluted with solid particle, instead of EPCM. The steady and unsteady performances of solar thermochemical reactor with non-uniform distribution of catalytic activity, in which catalyst is diluted with EPCM, are still unknown. What's more, the optimal catalytic activity distribution of solar thermochemical reactor for methanol steam reforming needs to be further explored.

The overall objective of this paper is to alleviate the adverse effect of solar radiation fluctuation on solar thermochemical reactor with encapsulated phase change material. Specific objectives are to explore the steady and dynamic behavior of solar thermochemical reactor diluted with encapsulated phase change material, and then optimize the distribution of catalytic activity in solar reactor. To achieve these goals, in this paper, at first, a two-dimensional dynamic model is established and validated with experimental data. Then, thermal and chemical performance of solar thermochemical reactor uniformly diluted with EPCM under steady and unsteady conditions of solar radiation are comprehensively analyzed. Afterwards, to better utilize the catalyst in chemical reactor, effect of non-uniform distribution of catalytic activity on steady-state chemical performance of solar chemical reactor is analyzed. Furthermore, for the high-accuracy and time-saving prediction of the chemical performance for solar thermochemical reactor, a one-dimensional model which is simplified from two-dimensional model with reasonable assumptions is used to train the Back Propagation neural network. Finally, the catalytic activity distribution of catalyst in solar chemical reactor is optimized by genetic algorithm and Back Propagation neural network, and steady and dynamic behaviors of solar chemical reactor with uniform and optimal catalytic activity distribution are comprehensively compared.

2. Model

2.1 Physical model

Fig. 1 illustrates the structure of solar parabolic trough receiver reactor (SPTRR) filled with mixture bed of catalyst and encapsulated phase change material (EPCM). As shown in Fig. 1, the SPTRR consists of receiver tube, catalyst and EPCM. In present paper, the LS2 solar parabolic trough receiver [31] is employed to concentrate solar radiation and generate heat for the chemical reaction. The catalyst used for methanol steam reforming reaction is $Cu/ZnO/Al_2O_3$ [32] and is diluted with encapsulated phase change material (EPCM) of $Sn@SiO_2$[26], in which Sn is core material serving as phase change material and SiO_2 is the shell material with good inert[18]. Thermophysical properties of catalyst and EPCM are listed in Table 1. The outer and inner diameter of receiver tube are 0.07 and 0.066 m, respectively, and the length is 5 m[31]. The tube is made of stainless steel 310S. The density, specific heat and thermal conductivity of 310S respectively is 8 $g\cdot cm^{-3}$, 500 $J\cdot kg^{-1}\cdot K^{-1}$ and 14.2 $W\cdot m^{-1}\cdot K^{-1}$.

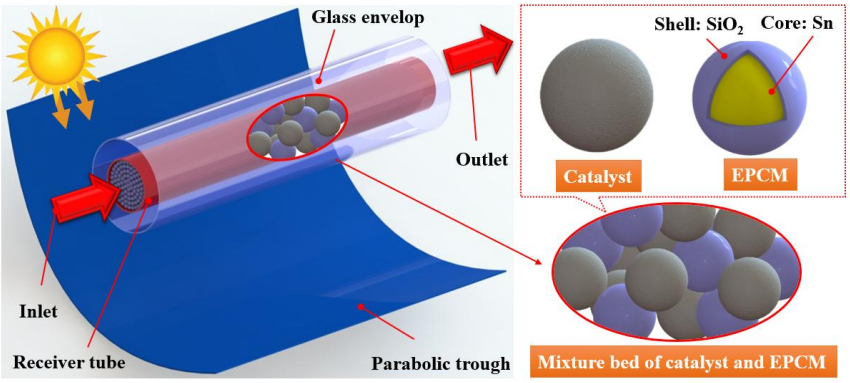

Fig. 1 Schematic diagrams of SPTRR diluted with EPCM

Table 1 Thermo-physical properties of catalyst and EPCM

Property	Value	Property	Value
Catalyst[33]		EPCM (Sn @ SiO_2)[18]	
ρ_{cat} /kg·m^{-3}	1300	ρ_{EPCM} /kg·m^{-3}	7184
$c_{p,cat}$ /J·kg^{-1}·K^{-1}	542	$c_{p,EPCM}$ /J·kg^{-1}·K^{-1}	244
λ_{cat} /W·m^{-1}·K^{-1}	20	$\lambda_{p,EPCM}$ / W·m^{-1}·K^{-1}	67
ε_{cat} and ε_{EPCM}	0.4	T_m/ K	505
		ΔT_m /K	2
		L_{EPCM}/ J·kg^{-1}	60500

In chemical reactor, reactants (methanol and steam both in vapor state) flow through reactor tube,

heated by solar radiation, undergoes chemical reaction on the surface of catalyst and are converted to hydrogen, carbon dioxide and carbon monoxide.

The concentrated solar radiation is non-uniformly distributed on the surface of reactor tube, but its effect on solar chemical reactor is negligible, which is indicated in ref. [34]. Meanwhile, some methods can be employed to largely improve the uniformity of solar radiation on reactor tube, such as[35] adding secondary reflector[36], variable focus parabolic trough[37], distribution optimization of solar absorption in receiver[38] and optimization of aiming strategy[39]. Herein, it is reasonable to assume that solar radiation is uniformly distributed on the surface of solar chemical reactor tube. Besides, some other assumptions are made to establish computational model as follows.

(1) The inlet mass flow rate and temperature of reactants (methanol and steam) are constant.

(2) The reactants (methanol and steam) and reaction productions (hydrogen, carbon dioxide and carbon monoxide) can be treated as ideal gas[33].

(3) Catalyst and EPCM are in same size[30], and the mixture of catalyst and EPCM bed is treated as isotropic porous media.

(4) The fluid phase and solid phase in chemical reactor are in local thermal equilibrium[18].

Using catalytic activity σ, the volume ratio f_{EPCM} of EPCM to mixture can be calculated[27] by:

$$f_{\mathrm{EPCM}} = 1-\sigma \tag{1}$$

where, σ is the catalyst activity.

Thus, thermo-physical properties of the mixture of catalyst EPCM can be calculated by following Equations [18, 27]:

$$\rho_{\mathrm{mix}} = \sigma\rho_{\mathrm{cat}} + \left(1-\sigma\right)\rho_{\mathrm{EPCM}} \tag{2}$$

$$\theta_{\mathrm{mix}} = \frac{\rho_{\mathrm{cat}}}{\rho_{\mathrm{cat}}+\rho_{\mathrm{EPCM}}}\theta_{\mathrm{cat}} + \frac{\rho_{\mathrm{EPCM}}}{\rho_{\mathrm{cat}}+\rho_{\mathrm{EPCM}}}\theta_{\mathrm{EPCM}} \tag{3}$$

where θ represents the thermal conductivity and specific heat of the mixture bed.

2.2 Governing equation

The computational domain contains two parts: mixture bed of catalyst and EPCM and reactor tube, which is illustrated in Fig. 2. Because SPTRR is axial symmetry, two-dimensional model is

employed. Governing equations of each part are displayed as follows.

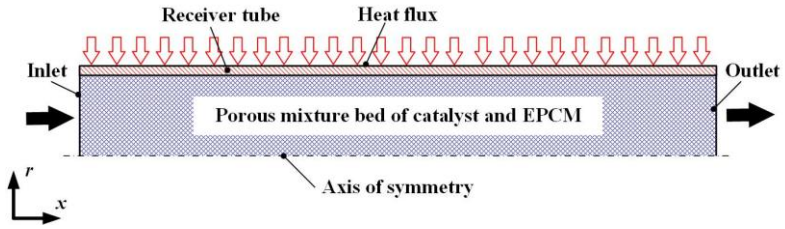

Fig. 2 Computational domain of SPTRR in which the catalyst is mixed with EPCM

2.2.1 The porous mixture bed of catalyst and EPCM:

Governing equations of the porous mixture bed include continuity equation, momentum equation, specie equation and energy conversation equation, which can be expressed as follows.

The continuity equation:

$$\frac{\partial\left(\varepsilon_{\text{mix}}\rho\right)}{\partial t}+\nabla\cdot\left(\varepsilon_{\text{mix}}\rho\vec{u}\right)=0 \tag{4}$$

where ε_{mix} represents the porosity of the porous mixture bed.

The momentum equation:

$$\frac{\partial\left(\varepsilon_{\text{mix}}\rho\vec{u}\right)}{\partial t}+\nabla\cdot\left(\varepsilon_{\text{mix}}\rho\vec{u}\vec{u}\right)=-\varepsilon_{\text{mix}}\nabla p+\nabla\cdot\left[\varepsilon_{\text{mix}}\left(\mu_{\text{t}}+\mu\right)\left(\frac{\partial u_i}{\partial x_j}+\frac{\partial u_j}{\partial x_i}\right)-\frac{2}{3}\varepsilon_{\text{mix}}\left(\mu_{\text{t}}+\mu\right)\delta_{ij}\nabla\cdot\vec{u}\right]+\vec{S}_i \tag{5}$$

where μ_{t} and μ are, respectively, the turbulent and dynamic viscosity of flow fluid, $\vec{S}_i$ represents momentum source term. The dynamic viscosity μ can be obtained in Ref. [40]. The source term of momentum equation can be can be found in Ref. [33].

The species conservation equation for each specie *i* can be depicted as:

$$\frac{\partial\left(\rho m_i\right)}{\partial t}+\nabla\cdot\left(\rho\vec{u}m_i\right)=\nabla\cdot\left[\left(\rho D_{m,i}+\frac{\mu_{\text{t}}}{Sc_{\text{t}}}\right)\nabla m_i\right]+Y_i \tag{6}$$

where m_i and $D_{m,i}$, respectively, are mass fraction and mass diffusion coefficient of specie *i*, Sc_{t} represents Schmidt number, which is set to be 0.7[31] in present study. Y_i is the source term for chemical reaction of specie *i* and its expression can be found in our prior work[41].

Reactions occurring in the porous mixture bed of catalyst and EPCM bed mainly contains 3 different chemical processes: methanol steam reforming reaction (MSR), methanol decomposition reaction (MDR), and water–gas shift reaction (WSR), which are expressed as follows:

$$CH_3OH + H_2O \rightleftharpoons CO_2 + 3H_2 \tag{7}$$

$$CH_3OH \rightleftharpoons CO + 2H_2 \tag{8}$$

$$CO + H_2O \rightleftharpoons CO_2 + H_2 \tag{9}$$

The comprehensive chemical kinetic model of methanol steam reforming model proposed by Peppley et al[32] is employed in this paper, which are shown in Eq. (10) - (12).

$$R_R = \frac{\sigma k_R K_{CH3O_{(1)}} \frac{p_{CH3OH}}{p_{H_2}^{1/2}} \left(1 - \frac{p_{H_2}^3 p_{CO_2}}{K_R p_{CH_3OH} p_{H_2O}}\right) C_{S1} C_{S1a} S_g}{\left(1 + K_{CH_3O_{(1)}} \frac{p_{CH_3OH}}{p_{H2}^{1/2}} + K_{HCOO} p_{CO_2} p_{H_2}^{1/2} + K_{OH_{(1)}} \frac{p_{H_2O}}{p_{H_2}^{1/2}}\right)\left(1 + K_{H_{(1)}}^{1/2} p_{H_2}^{1/2}\right)} \tag{10}$$

$$R_D = \frac{\sigma k_D K_{CH3O_{(2)}} \frac{p_{CH3OH}}{p_{H_2}^{1/2}} \left(1 - \frac{p_{H_2}^2 p_{CO}}{K_D p_{CH_3OH}}\right) C_{S2} C_{S2a} S_g}{\left(1 + K_{CH_3O_{(2)}} \frac{p_{CH_3OH}}{p_{H2}^{1/2}} + K_{OH_{(2)}} \frac{p_{H_2O}}{p_{H_2}^{1/2}}\right)\left(1 + K_{H_{(2)}}^{1/2} p_{H_2}^{1/2}\right)} \tag{11}$$

$$R_W = \frac{\sigma k_W K_{OH_{(1)}} \frac{p_{CO} p_{CH3OH}}{p_{H_2}^{1/2}} \left(1 - \frac{p_{H_2} p_{CO_2}}{K_W p_{CO} p_{H_2O}}\right) C_{S1}^2 S_g}{\left(1 + K_{CH_3O_{(1)}} \frac{p_{CH_3OH}}{p_{H2}^{1/2}} + K_{HCOO} p_{CO_2} p_{H_2}^{1/2} + K_{OH_{(1)}} \frac{p_{H_2O}}{p_{H_2}^{1/2}}\right)^2} \tag{12}$$

where σ represents the catalytic activity of the porous mixture ranging from 0 to 1, R_R, R_D and R_W are the reaction rate of MSR, MDR and WSR, respectively, p_i represents the partial pressure of specie i, C_{S1} and C_{S2}, respectively, are the concentration of active site S1 and S2 on the catalyst surface, S_g presents the surface area of catalyst. These detailed parameters can be found in our prior work[41].

The molar consumption rate of CH_3OH R_{CH_3OH} (in unit of $mol \cdot m^{-3} \cdot s^{-1}$) can be obtained by Eq. (13).

$$R_{CH_3OH} = -\left(R_R + R_D\right) \tag{13}$$

The energy conservative equation in the mixture bed of catalyst EPCM, based on the local thermal equilibrium, is given by:

$$\frac{\partial\left[\varepsilon_{mix}\rho_f c_{p,f} T + \left(1-\varepsilon_{mix}\right)\rho_{mix} c_{p,mix} T\right]}{\partial t} + \nabla\cdot\left(\rho_f c_{p,f} \vec{u} T\right) = \nabla\cdot\left(\lambda_{eff}\nabla T\right) + S_t \tag{14}$$

where the energy source term S_t can be found in our prior work[41].

In present study, the "effective heat capacity method" is employed to calculate the specific heat of EPCM during phase transition[18], which is shown in Eq. (15)

$$c_{p,\mathrm{EPCM,eff}} = \begin{cases} c_{p,\mathrm{EPCM}}, & T < T_\mathrm{m} - \dfrac{\Delta T}{2} \\ c_{p,\mathrm{EPCM}} + \dfrac{L_\mathrm{EPCM}}{\Delta T}, & T_\mathrm{m} - \dfrac{\Delta T}{2} \le T < T_\mathrm{m} + \dfrac{\Delta T}{2} \\ c_{p,\mathrm{EPCM}}, & T \ge T_\mathrm{m} + \dfrac{\Delta T}{2} \end{cases} \tag{15}$$

where ΔT is set to 2 K in this study[18].

2.2.2 The receiver tube:

The energy conversion equation describing heat conduction in the reactor tube is given by:

$$\frac{\partial \left(\rho c_p T\right)_\mathrm{tube}}{\partial t} = \nabla \cdot \left(\lambda_\mathrm{tube} \nabla T\right) \tag{16}$$

where λ_tube is the thermal conductivity of reactor tube.

2.3 Boundary condition

As illustrated in the Fig. 2, the boundary conditions of the simulation domain can be shown as follows:

(1) For porous mixture of catalyst and EPCM, the inlet and outlet boundaries are expressed as:

Inlet boundary: molar of molar ratio of H_2O/CH_3OH is set to 1.1, and temperature and flow velocity are constant, namely $u=u_\mathrm{in}$, $T=T_\mathrm{in}$=423.15 K, M_{H2O}/M_{CH3OH}=1.1.

Outlet boundary: the outlet pressure keeps constant, namely $p=p_\mathrm{out}$=101325 Pa.

(2) For the reactor tube region, the end surfaces of tube are constrained as adiabatic walls: $\partial T/\partial x = 0$.

(3) The boundary for axis of symmetry is expressed as: $\dfrac{\partial \vec{u}}{\partial r} = \dfrac{\partial T}{\partial r} = 0$

(4) The interface of tube region and mixture region is defined as the coupled fluid–solid interface, namely, $\vec{u} = 0$, $T_\mathrm{cat} = T_\mathrm{tube}$.

(5) In this study, the average local concentration ratio of solar collector is set to 20[31], and the direct normal irradiance (DNI) is assumed to be 600 $W \cdot m^{-2}$, herein, thus the heat flux on the surface of reactor tube is equal to 12000 $W \cdot m^{-2}$.

2.4 Definition of performance indicator

In present paper, the steady and unsteady performance of SPTRR are both investigated, thus some performance indicators are defined.

For steady condition of solar radiation, the performance of SPTRR is evaluated by methanol conversion efficiency η_c, which is expressed as:

$$\eta_c = \frac{\dot{m}_{CH_3OH,in} - \dot{m}_{CH_3OH,out}}{\dot{m}_{CH_3OH,in}} \tag{17}$$

where $\dot{m}_{CH_3OH,in}$ and $\dot{m}_{CH_3OH,out}$, respectively, represent the inlet and outlet mass flow rate of chemical reactor.

Due the weather transients, the solar radiation variation with time can be roughly divided into two different kinds: single-step fluctuation and successive fluctuation. Fig. 3 illustrates the illustration of two different typical solar radiation fluctuations. Thus, in present paper, for unsteady condition of solar radiation, Delay response time $\Delta t_{50,\eta_c}$ [42] and relatively vibrating amplitude of methanol conversion efficiency γ_{η_c} are adopted for the dynamic performance evaluation of SPRR under the single-step and successive fluctuations of solar radiation respectively.

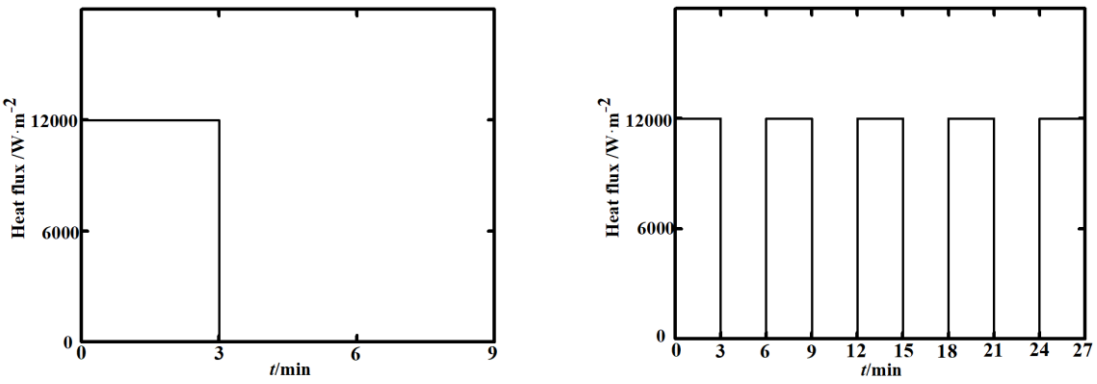

(a) Single step fluctuation (b) Successive step fluctuation

Fig. 3 Illustration of two different typical solar radiation fluctuations

Delay response time $\Delta t_{50,\eta_c}$ [42] is defined as the time during which the methanol conversion

efficiency changes by 50 % of $\Delta\eta_{c,total}$, which is illustrated in Fig. 4 And $\Delta\eta_{c,total}$ is total change of methanol conversion efficiency due to the step fluctuation of solar radiation. $\Delta t_{50,\eta_c}$ can reflect the ability of solar chemical reactor to delay the adverse effect of single fluctuation of solar radiation.

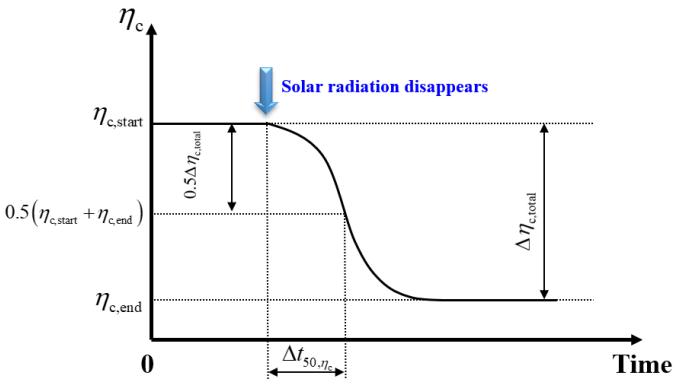

Fig. 4 Graphic illustration of delay response time $\Delta t_{50,\eta_c}$

The relatively vibrating amplitude of methanol conversion efficiency γ_{η_c} is defined as ratio of the vibrating amplitude value and time-average value of methanol conversion efficiency after solar chemical reactor reaches the repeatable state under successive fluctuations of solar radiation, and can be expressed as:

$$\gamma_{\eta_c}=\frac{\left(\eta_{c,max}-\eta_{c,min}\right)/2}{\eta_{c,ave}} \tag{18}$$

where $\eta_{c,max}$, $\eta_{c,min}$ and $\eta_{c,ave}$ are, respectively, the maximum, minimum and time-average value of methanol conversion efficiency during one repeatable cycle. And γ_{η_c} can reveal the stability of solar chemical reactor under successive fluctuations of solar radiation.

2.5 Numerical method and model validation

The governing equations described above are solved by Finite Volume Method, and the convective terms in momentum, species and energy conversion equations are discretized by second upwind scheme. SIMPLE algorithm[43] is employed to couple the velocity and pressure. Computational Fluid Dynamics (CFD) software FLUENT is used to solve the governing equations. The methanol conversion efficiency and outlet temperature calculated by four different grid systems

(i.e., 2500(x) ×18(r), 3333×23, 5000×35, 10000×70) are compared to exam the gird independence and the results are shown in Fig. 5 (a). As can be seen, the difference of predicted results including methanol conversion efficiency and outlet temperature between the grid systems of 5000(x)×35(r) and 10000(x)×70(r) is negligible, thus the gird system of 5000(x)×35(r) is adequate for predicting the thermal and chemical performance of SPTRR and adopted in following simulations. As for the independence test of time step, results calculated by four different time steps ranging from 0.5s to 5s are compared, which are illustrated in Fig. 5 (b). It can be seen that, the difference of methanol conversion efficiency variation curve with time predicted by 1s and 2s are quite close, and the time step of 2s is used in simulations for its sufficient accuracy and acceptable computational cost.

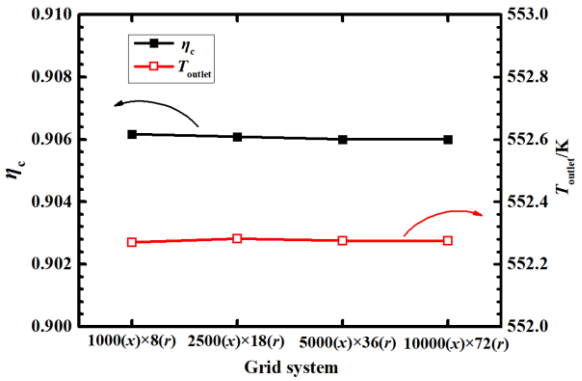

(a) Independence test of grid system

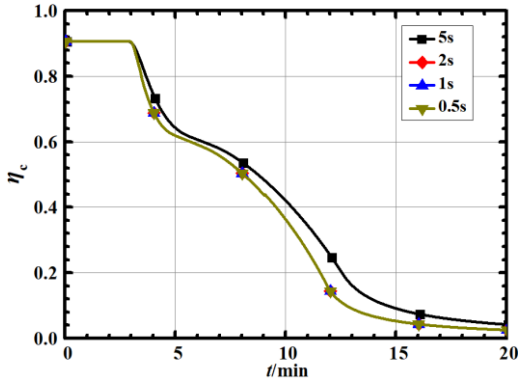

(b) Time-step independence test(Variation of methanol conversion efficiency with time)

Fig. 5 Grid and time-step independence test

The validation result of model can be found in our previous paper, which shows the model established is accurate enough to predict the performance of SPTRR.

3. Results and discussion

3.1 Thermal and chemical performance of SPTRR with uniform distribution of catalytic activity

In this section, the thermal and chemical performance of SPTRR with different catalytic activities under steady and unsteady condition of solar radiation are analyzed. In simulations, the inlet mass flow rate of reactants is equal to 0.01 kg·s^{-1}. The heat flux on the outer surface of reactor is set to 12000 W·m^{-2} for steady condition of solar radiation and varies with time for unsteady condition of solar radiation as illustrate in Fig. 3.

3.1.1 Thermal and chemical performance of SPTRR under steady condition of solar radiation

Fig. 6 (a) and (b) present the cross-sectional averaged temperature and molar consumption rate of CH_3OH variation along the flow direction for different catalytic activities, respectively. As can be seen from Fig. 6 (a), when x is smaller than 0.5 m, the cross-sectional averaged temperature of flow fluids increases rapidly along the flow direction due to the heat flux on the surface of reactor tube. Then, the rising rate of temperature is slower and keeps constant because of the high reaction rate of endothermic methanol steam reforming reaction, as is shown in Fig. 6 (b). And when x is larger than 4 m, the increasing rate of temperature is elevated again which is leaded by the decreasing of reactants' concentration and reduced reaction rate. For SPTRR with different catalytic activities, as catalytic activity decreases, the temperature at same position of x is improved and the highest consumption rate of CH_3OH in SPTRR is lower, indicating that more solar energy is converted to the sensible heat of reactants and productions instead of chemical energy.

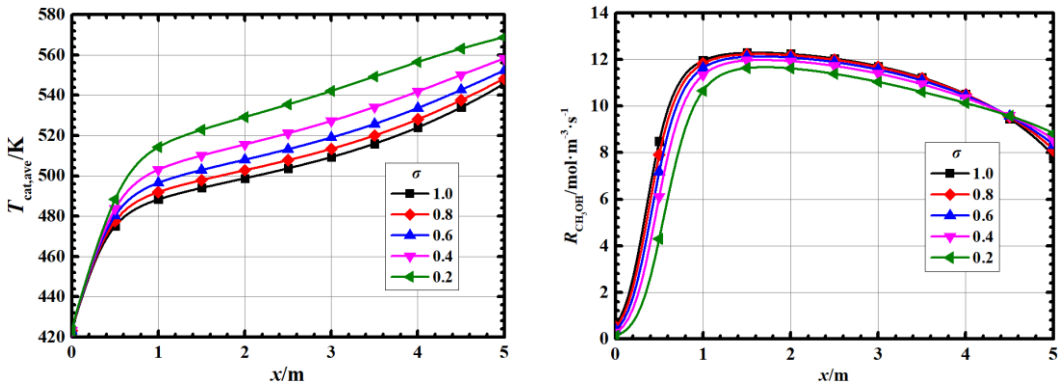

(a) Average temperature (b) Molar consumption rate of CH_3OH

Fig. 6 Cross-sectional averaged temperature and molar consumption rate of CH_3OH variation along the fluid direction for different catalytic activities

To avoid the sintering failure of catalyst and keep the safe operation of SPTRR, the reactor should be operating below the upper temperature limit of catalyst $Cu/ZnO/Al_2O_3$ (573 K). Fig. 7 presents thermal and chemical performance of SPTRR with different catalytic activities under steady condition. As can be seen from this figure that, as the catalytic activity decreases from 1.0 to 0.2, the maximum temperature of catalyst increases from 552 to 573 K, which is within the allowable temperature range of $Cu/ZnO/Al_2O_3$ catalyst for safe operation[32]. As for the chemical performance, it can be seen that, with the decrease of catalytic activity, the methanol conversion efficiency and

production rate of H_2 are both gradually reduced due to the decline of reaction rate, while production rate of CO is improved a lot due to the higher reaction rate of methanol decomposition reaction which produces CO. When catalytic activity decreases from 1.0 to 0.2, methanol conversion efficiency and $\dot{m}_{H_2}$ are reduced by 8.4 % and 9.9 % respectively, while $\dot{m}_{CO}$ rises by 121.3 %

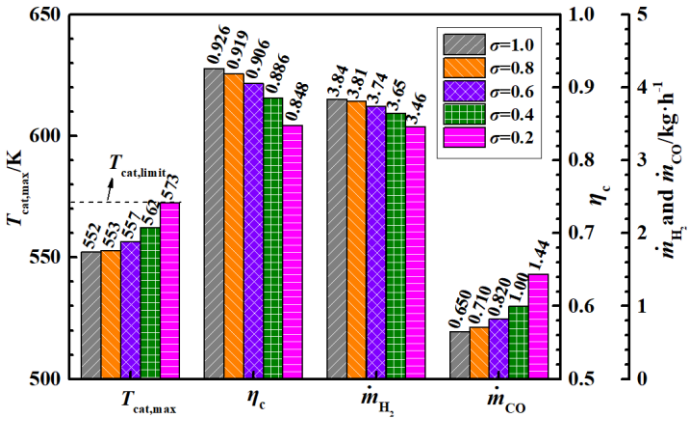

Fig. 7 Thermal and chemical performance of SPTRR with different catalytic activities under steady condition

3.1.2 Thermal and chemical performance SPTRR with under unsteady condition of solar radiation

In this section, the dynamic behavior of SPTRR with different catalytic activities are analyzed. There are two different types of solar radiation fluctuations: single step fluctuation and successive step fluctuation. In simulations, the nominal heat flux on the surface of reactor is 12000 W·m^{-2}. For the singe step fluctuation of solar radiation, the heat flux on the surface of reactor tube drops from 12000 W·m^{-2} to zero after t is larger than 3 min, as is shown Fig. 3 (a). For the successive step fluctuation of solar radiation, the heat flux switches between 12000 W·m^{-2} and zero for every 3 mins, which is illustrated in Fig. 3 (b).

(1) Single-step fluctuation of solar radiation

Fig. 8 (a) and (b) show $T_{cat,ave}$ and η_c variation with time of SPTRR with different catalytic activities under single step fluctuation of solar radiation, respectively. Clearly, when σ=1.0 (catalyst is not diluted with EPCM), after solar radiation disappears at t=3min, $T_{cat,ave}$ and η_c both decrease rapidly at first due to the short of heat supply, and then gradually reaches a stable value. While for σ

lower than 1.0 (catalyst is diluted with EPCM), compared with σ=1, the decreasing process of $T_{\mathrm{cat,ave}}$ and η_{c} after the disappearance of solar radiation is slower, and there exists a turning point in their decreasing processes due to the large latent heat released by EPCM. It can also be found that as σ declines, the turning point of $T_{\mathrm{cat,ave}}$ is higher, while the turning point of η_{c} decreases gradually. This phenomena can be explained by the fact that when the catalytic activity decreases, which means catalyst is diluted by more EPCM, the reaction rate at the same temperature decreases thus the turning point of methanol conversion efficiency declines. Meanwhile, with lower catalytic activity and higher filling proportion of EPCM in SPTRR, more latent heat can be released for endothermic chemical reactions (MSR and MD) in the temperature decreasing process, and temperature decreases slower, thus chemical reactions keeps lower methanol conversion efficiency at higher temperature for longer time. When the catalytic activity σ is diluted from 0.8 to 0.2, the turning value of η_{c} decreases from 0.72 to 0.38 greatly, which is reduced by 47.2 %.

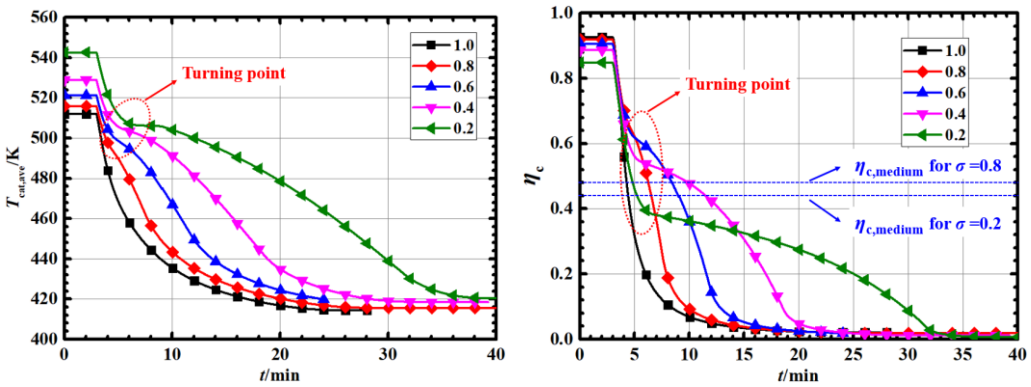

(a) Average temperature of catalyst (b) Methanol conversion efficiency

Fig. 8 $T_{\mathrm{cat,ave}}$ and η_{c} variation with time of SPTRR with different catalytic activities under single step fluctuation of solar radiation

Fig. 9 shows influence of catalytic activity on delay response time of SPTRR under step fluctuation of solar radiation. As can be seen in this figure, with the decreasing of σ from 1.0 to 0.2, $\Delta t_{50,\eta_{\mathrm{c}}}$ increases at first and reaches the maximum value of 8.2 mins at σ=0.4, then declines. This phenomena is caused by the reason that as σ decreases from 1.0 to 0.4, the content of EPCM in SPTRR becomes larger and the decreasing rate of methanol conversion efficiency is slower. However,

when σ is equal to 0.2, the turning point of methanol conversion efficiency in the decreasing process is lower than $\eta_{c,medium}$ (0.428, as shown in Fig. 8 (b)), therefore, the increasing of thermal inertia caused by EPCM makes little contribution to improvement of delay response time $\Delta t_{50,\eta_c}$. Compared with SPTRR fully packed with catalyst (σ=1), when σ is equal to 0.4, $\Delta t_{50,\eta_c}$ of SPTRR under step fluctuation of solar radiation is prolonged by 845 %, which means longer response time and can leave longer time for control system to make response.

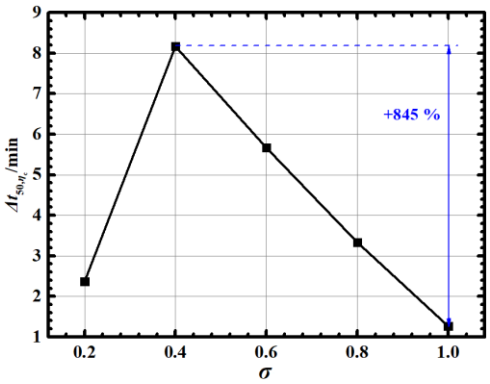

Fig. 9 Influence of catalytic activity on $\Delta t_{50,\eta_c}$ of SPTRR under step fluctuation of solar radiation

(2) Successive fluctuations of solar radiation

When the methanol conversion efficiency is relatively low (less than 0.3), the following process of separation and purification after reaction, such as pressure swing adsorption[11], will consumes lots of energy, which damages the economy of solar thermochemical reaction system. Similar with ref[13], in present paper the lowest limit of methanol conversion efficiency is set to 0.3.

Fig. 10 (a) shows the η_c variation with time of SPTRR for different catalytic activities under successive fluctuations of solar radiation. From Fig. 8 (a), it can be seen that η_c of SPTRR vibrates with the fluctuation of solar radiation, and finally can reach a repeatable state. Clearly, compared with SPTRR fully packed with EPCM (σ= 1.0), when catalyst is diluted with EPCM (σ= 0.2 and 0.6), the vibration amplitude of η_c is smaller, and the lowest value of η_c in the vibrating process is also improved after SPTRR reaches a repeatable state. For example, compared with σ= 1.0, when σ is diluted by EPCM to 0.2, the lowest value of η_c in a repeatable cycle is improved from 0.192 to 0.328, which is higher than lowest limit of methanol conversion efficiency (0.3) and can avoid the

sudden shut down of chemical reaction system. Fig. 8 (b) illustrates average value and relative vibrating amplitude of η_c after SPTRR reach repeatable state. Clearly, when catalyst is diluted by EPCM and σ decreases from 1.0 to 0.2, $\eta_{c,ave}$ increases at first and reaches maximum of 0.459 at σ=0.4, and then decreases due to its low catalytic activity, meanwhile, γ_{η_c} declines rapidly initially and reaches the lowest value of 0.223 at σ=0.4 due to its large thermal inertia. Compared with σ=1.0, the average value and relatively vibrating amplitude of methanol conversion efficiency in SPTRR with σ=0.4 are, respectively, prompted by 11.7 % and reduced by 69.8 %, which shows better stability of SPTRR under successive step fluctuation of solar radiation.

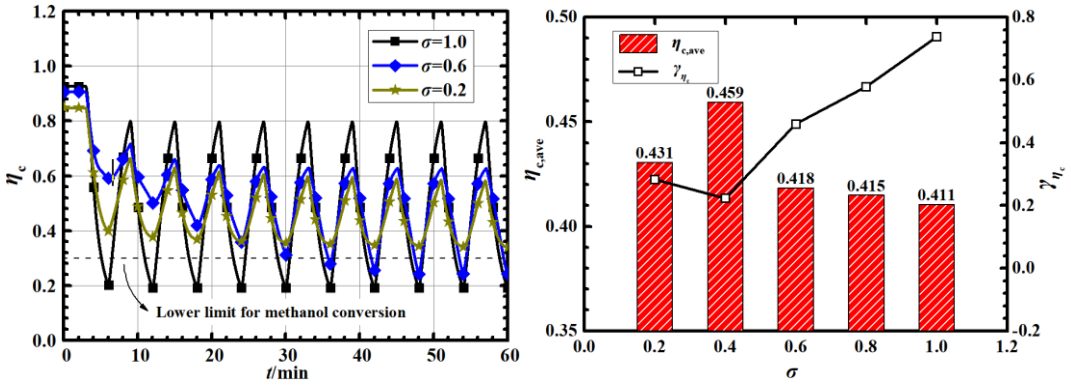

(a) Methanol conversion efficiency

(b) $\eta_{c,ave}$ and γ_{η_c}

Fig. 10 Variation and relatively vibrating amplitude of η_c in SPTRR with different catalytic activities under successive fluctuations of solar radiation

3.2 Chemical performance of SPTRR with non-uniform distribution of catalytic activity

As mentioned above, when catalyst is diluted with large amount of EPCM, the unsteady performance of STPRR can be greatly improved. However, due to the decrease of catalytic activity, the chemical performance of SPTRR under steady solar radiation, such methanol conversion efficiency, declines. To achieve high steady performance and stable dynamic behavior at the same time, non-uniform distribution of catalytic activity is applied in SPTRR. In this section, the chemical performance of SPTRR with 2-part distribution of catalytic activity, which is shown in Fig. 11, is analyzed. σ_1 and σ_2 are the catalytic activity at the front and end part of reactor respectively.

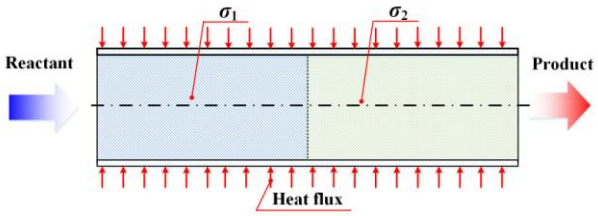

Fig. 11 Illustration of 2-part SPTRR with different catalytic activities

Fig. 12 depicts the methanol conversion efficiency of SPTRR with 2-part distribution of catalytic activity under steady condition. It is found that when the front-part catalytic activity σ_1 is constant, with the increasing of end-part catalytic activity σ_2, the methanol conversion efficiency of SPTRR is improved gradually. Correspondingly, it should be noted that, on the condition that σ_2 is constant, the effect of σ_1 on methanol conversion efficiency of SPTRR highly depends on the value of σ_2. That is, when σ_2 keeps equal to 0, improvement of σ_1 can lead to the uprising of η_c. However, when σ_2 keeps larger or equal to 0.2, the variation of σ_1 has negligible effect on η_c of SPTRR. For example, when σ_2 is equal to 1.0, as σ_1 varies between in the range of 0.2 to 1.0, η_c of SPTRR changes very little from 0.924 to 0.926. Thus, it can be concluded that the effect of catalytic activity on η_c depends on the catalyst position in SPTRR. This phenomena is caused by the fact the catalyst temperature increases along with the flow direction, and with same catalytic activity, based on the Arrhenius equation[44], the reaction rate at the end part is much larger than that at the front part, thus the effect of catalytic activity's variation at the end part (σ_2) on methanol conversion efficiency is more prominent than that at front part. Therefore, in order to achieve efficient steady and unsteady performance at the same time, it is be a feasible way to keep high methanol conversion efficiency, low total catalytic activity (i.e. large amount of EPCM) and high thermal inertia simultaneously by properly adjusting the distribution of catalytic activity. For example, by adjusting the catalytic activity distribution form all catalyst ($\sigma_1=\sigma_2=1.0$) to distribution of $\sigma_1=0.2$ and $\sigma_2=1.0$, the methanol conversion efficiency keeps high level (drops by less than 0.4%) with 40% decline of average catalytic activity, indicating much less usage of catalyst and huge amount of EPCM with large thermal

inertia.

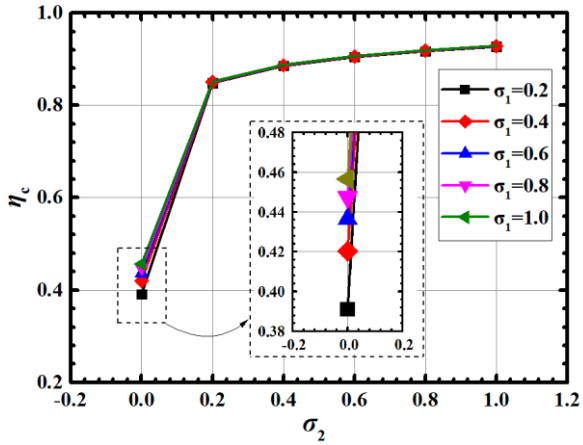

Fig. 12 Methanol conversion efficiency of SPTRR with 2-part distribution of catalytic activity

3.3 Distribution optimization of catalytic activity in SPTRR under steady condition of solar radiation

To achieve the efficient steady and unsteady performance of SPRR simultaneously, namely keeps high methanol conversion efficiency, high content of EPCM and low average catalytic activity at the same time, SPTRR is separated into 3 parts along the flow direction equally, and the catalytic activity of each part is optimized. Firstly, based on some reasonable assumptions, the two-dimensional model is simplified to one-dimensional model, which is validated by the results predicted by two-dimensional model. Then, the Back Propagation (BP) neural network is trained and validated with dataset calculated by 1-dimensional model for quick prediction of methanol conversion efficiency. Finally, using the trained BP neural network, the distribution of catalytic activity in SPTRR is optimized by Genetic Algorithm (GA), and chemical performance of SPTRR with optimized distribution of catalytic activity and fully packed with catalyst (σ=1) are compared.

3.3.1 Simplification of two-dimensional governing equation

To reduce the computational cost and keep high calculation precision at the same time, some assumptions are made to derive the 1-dimensional model from 2-dimensional model[30]:

(1) The concentration gradient of reactants and productions along the radial direction are negligible ($\partial m_i/\partial r$ = 0), because of the rapid diffusion of reactant and production along the radial

direction, and small radial concentration difference.

(2) The radial temperature gradient is considered in simulation because large amount of heat is absorb by the surface of reactor tube.

(3) The temperature distribution along radial direction can be approximated to parabolic curve. In present study, temperature profile along the radial direction is depicted as:

$$T(x,r)=\left[1+a\left(\frac{r}{R_{\text{reactor}}}\right)^2\right]T(x,0) \tag{19}$$

where, x and r represent the axial and radial coordinates, respectively, a is the coefficient related with the distribution profile of temperature, R_{reactor} represents the radius of chemical reactor.

To determine the temperature profile coefficient a of solar chemical reactor for methanol steam reforming reaction, radial temperature distributions of SPTRR are calculated by two-dimensional model, and the results are used to fit the temperature profile coefficient a by least square method. The obtained temperature profile coefficients for different catalytic activities which are shown in Table 2

Table 2 Distribution coefficient of radial temperature profile for different catalytic activities

σ	1.0	0.8	0.6	0.4	0.2	0
$a/\times10^{-3}$	28.196	11.328	9.1992	8.511	7.715	19.790

The average temperature of cross-sectional area can be derived by Eq. (20)

$$\overline{T}(x)=\frac{\int_0^{R_{\text{reactor}}}\left[1+a\left(\frac{r}{R_{\text{reactor}}}\right)^2\right]T(x,0)\cdot 2\pi r\mathrm{d}r}{\pi R_{\text{reactor}}^2}=\left(1+\frac{a}{2}\right)T(x,0) \tag{20}$$

Thus, the local temperature of SPTRR can be expressed with $\overline{T}(x)$, which can be derived by Eq. (21) using

$$T(x,r)=\frac{\left[1+a\left(\frac{r}{R_{\text{reactor}}}\right)^2\right]}{1+\frac{a}{2}}\overline{T}(x) \tag{21}$$

The one-dimensional models of species equation and energy conversation equation can be obtained by integrating Eq. (6)and Eq. (14) along the cross-sectional area of SPTRR, which are expressed in Eq. (23) and Eq. (22).

$$\frac{\partial(\rho m_i)}{\partial t}+\nabla\cdot(\rho u m_i)=\nabla\cdot\left[\left(\rho D_{m,i}+\frac{\mu_t}{Sc_t}\right)\nabla m_i\right]+F\cdot\sigma M_{w,i}\sum_{r=1}^{N_R}\hat{R}_{i,r}\left(\overline{T}\right) \tag{22}$$

$$\frac{\partial\left(\rho c_p\overline{T}\right)}{\partial t}+\nabla\cdot\left(\rho c_p u\overline{T}\right)=\lambda_{\text{eff}}\frac{\partial^2\left(\overline{T}\right)}{\partial x^2}+S_{\text{solar}}+F\cdot St\left(\overline{T}\right) \tag{23}$$

where the energy source term S_{solar} is caused by solar radiation and defined in Eq. (24), F is the correction coefficient for cross-sectional average reaction rate.

$$S_{\text{solar}}=\frac{2\pi R_{\text{reactor}}\cdot q}{\pi R_{\text{reactor}}^2} \tag{24}$$

According to Arrhenius Equation[44], the relation between reaction rate $R(T)$ and temperature can be expressed as[27]:

$$R(T)=R\left(\overline{T}\right)\exp\left[\frac{E}{R\overline{T}^2}\left(T-\overline{T}\right)\right] \tag{25}$$

Therefore, the correction coefficient F for cross-sectional average reaction rate can be derived by Eq. (26).

$$\begin{aligned}F&=\frac{\overline{R(T)}}{R\left(\overline{T}\right)}\\&=\frac{\int_0^{R_{\text{reactor}}}A\exp\left(\frac{E}{R\overline{T}}\right)\exp\left[\frac{E}{R\overline{T}^2}\left(T-\overline{T}\right)\right]\cdot 2\pi r\mathrm{d}r\Big/\pi R_{\text{reactor}}^2}{A\exp\left(\frac{E}{R\overline{T}}\right)}\\&=\frac{R\overline{T}\left(1+\frac{a}{2}\right)}{Ea}\left\{\exp\left[\frac{Ea}{2R\overline{T}\left(1+\frac{a}{2}\right)}\right]-\exp\left[\frac{-Ea}{2R\overline{T}\left(1+\frac{a}{2}\right)}\right]\right\}\end{aligned} \tag{26}$$

where E is the activity energy for chemical reaction, and the values are shown in Table 3.

Table 3 Activity energy for different chemical reactions[32]

Reaction	MSR	MD	WSR
E/ J·mol^{-1}	102800	170000	87600

Fig. 13 compares temperature and methanol conversion efficiency calculated by 2-dimensional

and 1-dimensional model. From Fig. 13 (a), clearly, it can be seen that for different catalytic activities (σ=0.2, 0.4, 0.6, 0.8, 1.0), the cross-sectional average temperature variations along flow direction predicted by 1-dimenional model and 2-dimensional model are quite close. And as can be found in Fig. 13 (b) that, the deviation between methanol conversion efficiencies calculated by 1-dimensional and 2-dimensional model are relatively small, and the largest deviation is 0.21 %, and as for the maximum catalyst temperature, the largest discrepancy is below 0.5 % when the σ ranges from 0.2 to 1.0. Therefore, it can be concluded that 1-dimensional model is accurate enough to predict the thermal and chemical performance of SPTRR with different catalytic activities.

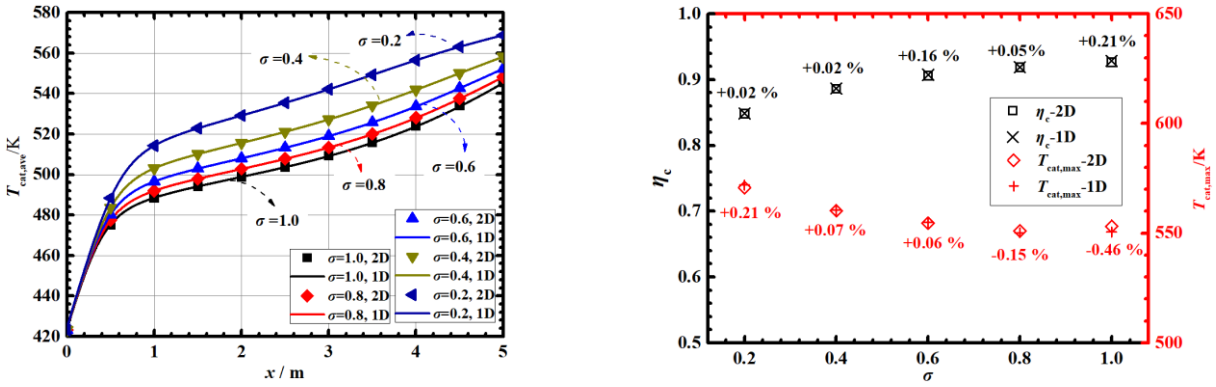

(a) Cross-sectional average temperature variation along flow direction

(b) Methanol conversion efficiency and max temperature of catalyst

Fig. 13 Comparison of results of temperature and methanol conversion efficiency calculated by two-dimensional and one-dimensional model

In addition, the comparison of computational cost between 1-dimensional and 2-dimensional model is performed on a computer with 8-core 2.3 GHz CPU and 32 GB RAM. For the case of SPTRR with catalytic activity of 0.8, the computing time of one-dimensional model is about 22 min for a steady condition case, which is much shorter than that of two-dimensional model (305 min). Therefore, it can be concluded that one-dimensional model is accurate enough and time-saving compared to two-dimensional model for simulating the heat transfer and chemical process of SPTRR，which is beneficial for quick performance prediction of SPTRR.

3.3.2 Distribution optimization of catalytic activity along axial direction

As mentioned above, the computing time of one-dimensional model for one case of SPTRR is

around 22 min, which is still relatively long to be applied for the optimization of catalytic activity distribution. To overcome this problem, BP (Back Propagation) neural network is adopted to predict the chemical performance of SPTRR with different catalytic activities, and one-dimensional model is employed to produce the training and validation data for the establishment and testing of BP neural network. The inputs of BP neural network are catalytic activities of each part (σ_1, σ_2 and σ_3), and output is methanol conversion efficiency. BP neural network is a multi-layer neural network, and has been widely applied in fields of image analysis and speech recognition due to its strong non-linear mapping ability, high self-learning and self-adaptive ability. Weights and thresholds during the signal transmission in BP neural network are key parameters for the accuracy of prediction, thus in present paper, genetic algorithm (GA) is used to optimize the training process of the neural network, and find optimal weights and thresholds that meet the requirements of the network. Table 4 lists the training and validation dataset for BP neural network, which contains 100 cases for neural net training, 32 cases for neural net validation and 16 cases for neural net testing.

Table 4 Training and validation dataset for BP neural network

Dataset	σ_1	σ_2	σ_3	Number of case
Training	0.2, 0.4, 0.8, 1.0	0, 0.2, 0.4, 0.6, 1.0	0, 0.2, 0.6, 0.8, 1.0	100
Validation	0.6	0.2, 0.4, 0.6, 1.0	0.2, 0.6, 0.8, 1.0	16
	0.2, 0.4, 0.8, 1.0	0.8	0.2, 0.6, 0.8, 1.0	16
Testing	0.2, 0.4, 0.8, 1.0	0.2, 0.4, 0.6, 1.0	0.4	16

Three-layer neural network is employed and the number of neurons in the hidden layer is set to 10. The trainlm function is used as training function, the upper number for training is 10000 and the convergence target is set to 1.0×10^{-7}. In genetic algorithm, the optimizing objective is shown in Eq. (27), and the parameters in optimization are listed in Table 5.

$$\min\left(\sqrt{\sum_{i=1}^{n}\left(\eta_{\mathrm{BP},i}-\eta_{\mathrm{validation},i}\right)^2}\right) \tag{27}$$

where $\eta_{\mathrm{BP},i}$ and $\eta_{\mathrm{validation},i}$ are methanol conversion efficiency predicted by BP neural network and from the validation dataset calculated by one-dimensional model, respectively, n is the number of case

in the validation dataset.

Table 5 Parameter in the optimizing process of genetic algorithm

Population size	Maximum generations	Binary digits of variable	Crossing probability	Mutation probability	Generation gap
100	100	10	0.7	0.01	0.95

Fig. 14 shows comparison of methanol conversion efficiency calculated by BP neural network and 2-D model. From this figure, it can be seen that the methanol conversion efficiency predicted by trained neural network matches well with the results calculated by 2-D model. Thus, the trained neural network can be used to predicting the methanol conversion efficiency of SPTRR with different catalytic activities.

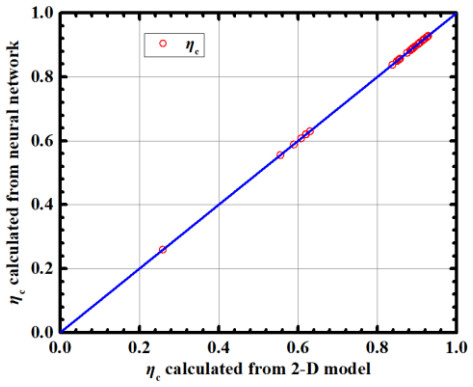

Fig. 14 Methanol conversion efficiency calculated from BP neural network and 2-D model

Furthermore, genetic algorithm is employed to optimize the distribution of catalytic activity along the flow direction based on the obtained BP neural network. In order to achieve efficient steady performance and stable dynamic behavior at the same time, i.e., high methanol conversion efficiency and low average catalytic activity, methanol conversion efficiency and average catalytic activity are combined as the optimization objective, which is defined as Eq. (28). To keep high methanol conversion efficiency and avoid the overshoot of catalyst temperature, the constraints on η_c and σ are considered, which are expressed as Eq. (29) and Eq. (30)

Optimization objective:

$$\mathrm{Max}\left(\eta_c \Big/ \left[\frac{(\sigma_1+\sigma_2+\sigma_3)}{3}\right]\right) \tag{28}$$

Constraints:

$$\eta_c > \eta_{c,0} \times 0.99 \tag{29}$$

$$0.2<\sigma_i<1,\ i=1,\ 2,\ 3 \tag{30}$$

where $\eta_{c,0}$ is the methanol conversion efficiency of SPTRR fully packed with catalyst.

The parameters of genetic algorithm for distribution optimization of catalytic activity are same with that for BP neural network, and the optimized distribution of catalytic activity by GA is listed in Table 6. As can be seen in this table, the optimized distribution of catalytic activity is σ_1=σ_1=0.2, σ_3=0.916 with the average catalytic activity of 0.44, and the predicted methanol conversion efficiency is 0.920.

Table 6 Optimal distribution of catalytic activity

σ_1	σ_2	σ_3	$\eta_{c,BP}$	$\eta_{c,2D}$	$\eta_{c,BP}\Big/\left[\frac{(\sigma_1+\sigma_2+\sigma_3)}{3}\right]$
0.2	0.2	0.916	0.920	0.919	2.097

Then, two-dimensional model is employed to calculate the methanol conversion efficiency of SPTRR with the optimal distribution of catalytic activity, and the calculated $\eta_{c,2D}$ is 0.919, which is relatively close to $\eta_{c,BP}$ (0.920) predicted by BP neural network, indicating that the predicted results by neural network are accurate and valid.

3.4 Steady and dynamic performance of SPTRR with optimal distribution of catalytic activity

After obtaining the optimal analytic activity distribution, in this section, the thermal and chemical performance of STRR filled with uniform and optimal distribution of analytic activity are compared and analyzed. In simulations, the results are calculated by 2-D model.

The maximum temperature of catalyst and methanol conversion efficiency of SPTRR with different catalytic activity distributions of $\sigma_{uniform}$=1, $\sigma_{uniform}$=0.44 and $\sigma_{optimal}$ are compared, which shown in Fig. 15 (a). It is found that for these three catalytic activity distributions, the highest temperatures of catalyst are all below the upper limit temperature of catalyst (573 K), which can ensure the safe and long-term run of SPTRR. Among these three catalytic activity distributions, SPTRR with $\sigma_{uniform}$=0.44 has the highest catalyst temperature of 560.9 K, then is SPTRR with

$\sigma_{uniform}$=1, and SPTRR with $\sigma_{optimal}$ has the lowest catalyst temperature of 549.5 K, indicating that SPTRR with $\sigma_{optimal}$ is farthest away from the catalyst limit temperature and can handle the sudden uprising of solar radiation best. For the chemical performance, although the average catalytic activity is 0.44, with 56 % less of catalyst, methanol conversion efficiency of SPTRR with $\sigma_{optimal}$ is similar with that of SPTRR fully packed with catalyst ($\sigma_{uniform}$=1), and larger than that of SPTRR with $\sigma_{uniform}$=0.44. It can be concluded that with much less catalyst and high content of EPCM, SPTRR with optimal distribution of catalytic activity can keep similar steady thermal and chemical performance with SPTRR with fully packed with catalyst.

Due to the low methanol conversion efficiency of SPTRR filled with $\sigma_{optimal=0.44}$ under steady condition of solar radiation, only dynamic behavior comparison of SPTRR with $\sigma_{uniform}$=1 and $\sigma_{optimal}$ under unsteady condition of solar radiation are compared, which is illustrated in Fig. 15 (b). Clearly, as can be seen from this figure, when SPTRR is under single step fluctuation of solar radiation, compared with $\sigma_{uniform}$=1, the delay response time $\Delta t_{50,\eta_c}$ of SPTRR with $\sigma_{optimal}$ is much prolonged from 1.3 mins to 2.8 mins, nearly improved by 115.4%. And when SPTRR is under the successive fluctuation of solar radiation, the relatively vibrating amplitude γ_{η_c} of SPTRR with $\sigma_{optimal}$ is largely alleviated from 0.78 to 0.32, which is almost reduced by 60 %, compared to that of SPTRR with $\sigma_{uniform}$=1. Therefore, it can be concluded that compared with $\sigma_{uniform}$=1, SPTRR with $\sigma_{optimal}$ has larger thermal inertia to leave more time for controller to take action and shows more stable dynamic behavior under the fluctuation of solar radiation.

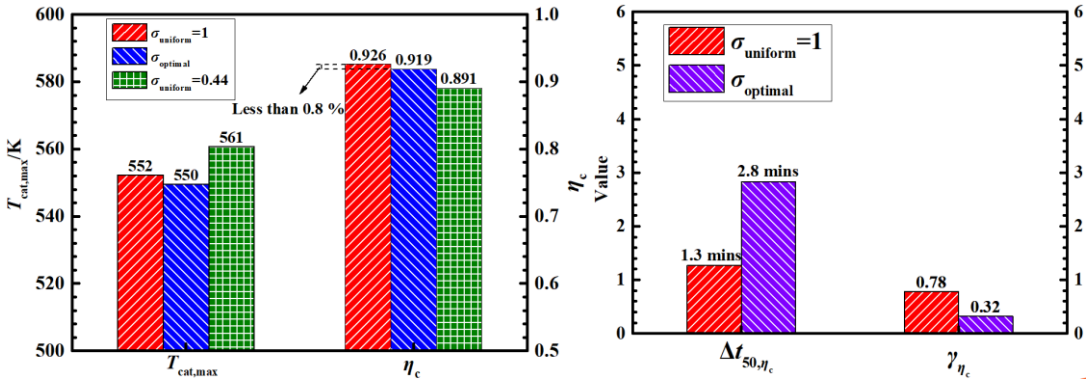

(a) Steady performance (b) Dynamic performance

Fig. 15 Steady and dynamic performance comparison of SPTRR with different distributions of catalytic activity

4. Conclusion

In this study, the catalytic activity of solar thermochemical reactor is adjusted by the diluting catalyst with EPCM to improve the steady and dynamic performance of SPTRR. At first, a two-dimensional model is established to compare steady performance of reactor with different catalytic activities. Then, one-dimensional model is derived from two-dimensional model and used to train BP neural network. Finally, optimal distribution of catalytic activity is obtained by genetic algorithm and BP neural network, and the steady and dynamic performance of SPTRR with uniform distribution and optimal distribution are compared. The salient findings are as follows:

(1) For steady performance of solar thermochemical reactor, when catalytic activity decreases from 1.0 to 0.2, the maximum temperature of catalyst increases from 552 to 573 K, which is still within the allowable temperature range of $Cu/ZnO/Al_2O_3$ catalyst for safe operation, and methanol conversion efficiency and $\dot{m}_{H_2}$ are reduced by 8.4 % and 9.9 % respectively, while $\dot{m}_{CO}$ rises by 121.3 %.

(2) For the dynamic performance, compared with solar thermochemical reactor fully packed with catalyst (σ=1), when σ is diluted by encapsulated phase change material to 0.4, $\Delta t_{50,\eta_c}$ of reactor under single-step fluctuation of solar radiation is prolonged by 845 % and relatively vibrating amplitude of methanol conversion efficiency is reduced by 69.8 %, which shows better stability.

(3) One-dimensional simplified model derived in present study is accurate enough and time-saving compared to two-dimensional model.

(4) With 56 % less of catalyst, solar thermochemical reactor with optimal distribution of catalytic activity can keep similar steady thermal and chemical performance with SPTRR fully packed with catalyst.

Acknowledgement

This research is supported by the National Natural Science Foundation of China (No. 51976156, 51906186).

The authors would also like to thank the Foundation for Innovative Research Groups of the National Natural Science Foundation of China (No.51721004) and the Foundation for San Qin Scholar Innovative Research Groups of Shaanxi Province.

Nomenclature and units

c_p	specific heat, $J \cdot kg^{-1} \cdot K^{-1}$
d_{cat}	diameter of catalyst particles, m
D	diameter, m
f_{EPCM}	volume ratio of EPCM to mixture
h_0	formation enthalpy, $J \cdot mol^{-1}$
k_{cat}	permeability of catalyst, m^2
k	turbulence kinetic energy, $m^2 \cdot s^{-2}$
L	latent heat, $J \cdot kg^{-1}$
L_{tube}	length of tube, m
$\dot{m}$	mass flow rate, $kg \cdot h^{-1}$
m_i	mass fraction of species i
M_i	mole fraction of species i
$M_{w,i}$	molecular weight of species i, $kg \cdot mol^{-1}$
n	molar flow rate, $mol \cdot s^{-1}$

$\hat{R}_{i,r}$	rates of creation and destruction of species *i* in the reaction *r*, $mol \cdot m^{-3} \cdot s^{-1}$
Sc_t	effective turbulent Schmidt number
t	time, s
T	temperature, K
p	pressure, Pa
Q	total heat transfer rate, W
R	universal gas constant, $J \cdot mol^{-1} \cdot K^{-1}$
R_R	reaction rate of methanol steam reforming reaction, $mol \cdot m^{-3} \cdot s^{-1}$
R_D	reaction rate of methanol decomposition reaction, $mol \cdot m^{-3} \cdot s^{-1}$
R_W	reaction rate of water shift reaction, $mol \cdot m^{-3} \cdot s^{-1}$
$\vec{u}$	velocity vector, $m \cdot s^{-1}$

Greek symbols

β	inertial loss coefficient, m^{-1}
γ_{η_c}	relatively vibrating amplitude of methanol conversion efficiency
$\Delta t_{50,\eta_c}$	delay response time of methanol conversion efficiency, s
δ_{ij}	Kronecker's delta
ε	turbulence kinetic energy dissipation rate, $m^2 \cdot s^{-3}$
ε_{mix}	porosity of packed mixture of catalyst and EPCM
η_c	methanol conversion efficiency
λ	thermal conductivity, $W \cdot m^{-1} \cdot K^{-1}$

μ	dynamic viscosity, Pa·s
μ_t	turbulent viscosity, Pa·s
ρ	density, kg·m^{-3}
σ	catalytic activity

Subscripts

ave	average
cat	catalyst
eff	effective
f	fluid
i	species
mix	mixture of catalyst and EPCM
s	solid

Abbreviations

DNI	direct normal irradiance
EPCM	Encapsulated phase change material
MD	methanol decomposition
MSR	methanol steam reforming
PCM	phase change material
SPTRR	solar parabolic trough receiver reactor

WSR	water–gas shift reaction

References

[1] Li MJ, Tao WQ. Review of methodologies and polices for evaluation of energy efficiency in high energy-consuming industry. Applied Energy. 2017;187:203-15.

[2] Yadav D, Banerjee R. A review of solar thermochemical processes. Renewable & Sustainable Energy Reviews. 2016;54:497-532.

[3] Wang YJ, Liu QB, Sun J, Lei J, Ju Y, Jin HG. A new solar receiver/reactor structure for hydrogen production. Energy Conversion and Management. 2017;133:118-26.

[4] Liu XF, Hong H, Jin HG. Mid-temperature solar fuel process combining dual thermochemical reactions for effectively utilizing wider solar irradiance. Applied Energy. 2017;185:1031-9.

[5] Hao Y, Jin J, Jin HG. Thermodynamic analysis of isothermal CO2 splitting and CO2-H2O co-splitting for solar fuel production. Applied Thermal Engineering. 2019;166:113600.

[6] Chuayboon S, Abanades S, Rodat S. Syngas production via solar-driven chemical looping methane reforming from redox cycling of ceria porous foam in a volumetric solar reactor. Chemical Engineering Journal. 2019;356:756-70.

[7] Romero M, Steinfeld A. Concentrating solar thermal power and thermochemical fuels. Energy & Environmental Science. 2012;5:9234-45.

[8] Liu QB, Wang YJ, Lei J, Jin HG. Numerical investigation of the thermophysical characteristics of the mid-and-low temperature solar receiver/reactor for hydrogen production. International Journal of Heat and Mass Transfer. 2016;97:379-90.

[9] Jiang Q, Zhang H, Deng Yn, Kang Q, Hong H, Jin H. Properties and reactivity of LaCuxNi1−xO3 perovskites in chemical-looping combustion for mid-temperature solar-thermal energy storage. Applied energy. 2018;228:1506-14.

[10] Iulianelli A, Ribeirinha P, Mendes A, Basile A. Methanol steam reforming for hydrogen generation via conventional and membrane reactors: a review. Renewable and Sustainable Energy Reviews. 2014;29:355-68.

[11] Liu QB, Hong H, Yuan JL, Jin HG, Cai RX. Experimental investigation of hydrogen production integrated methanol steam reforming with middle-temperature solar thermal energy. Applied Energy. 2009;86:155-62.

[12] Rowe SC, Hischier I, Palumbo AW, Chubukov BA, Wallace MA, Viger R, et al. Nowcasting, predictive control, and feedback control for temperature regulation in a novel hybrid solar-electric reactor for continuous solar-thermal chemical processing. Solar Energy. 2018;174:474-88.

[13] Saade E, Clough DE, Weimer AW. Model predictive control of a solar-thermal reactor. Solar Energy. 2014;102:31-44.

[14] Petrasch J, Osch P, Steinfeld A. Dynamics and control of solar thermochemical reactors. Chemical Engineering Journal. 2009;145:362-70.

[15] Roca L, de la Calle A, Yebra LJ. Heliostat-field gain-scheduling control applied to a two-step

solar hydrogen production plant. Applied energy. 2013;103:298-305.
[16] Muroyama A, Shinn T, Fales R, Loutzenhiser PG. Modeling of a dynamically-controlled hybrid solar/autothermal steam gasification reactor. Energy & Fuels. 2014;28:6520-30.
[17] Kuhn P, Wilbert S, Schüler D, Prahl C, Haase T, Ramirez L, et al. Validation of spatially resolved all sky imager derived DNI nowcasts. AIP conference proceedings: AIP Publishing; 2017. p. 140014.
[18] Odunsi AO, O'Donovan TS, Reay DA. Temperature stabilisation in Fischer-Tropsch reactors using phase change material (PCM). Applied Thermal Engineering. 2016;93:1377-93.
[19] Jiang G, Huang J, Liu M, Cao M. Experiment and simulation of thermal management for a tube-shell Li-ion battery pack with composite phase change material. Applied Thermal Engineering. 2017;120:1-9.
[20] Ma Z, Yang WW, Yuan F, Jin B, He YL. Investigation on the thermal performance of a high-temperature latent heat storage system. Applied Thermal Engineering. 2017;122:579-92.
[21] Huang YH, Cheng WL, Zhao R. Thermal management of Li-ion battery pack with the application of flexible form-stable composite phase change materials. Energy Conversion and Management. 2019;182:9-20.
[22] Pattison RC, Baldea M. A thermal - flywheel approach to distributed temperature control in microchannel reactors. AIChE journal. 2013;59:2051-61.
[23] Hatamachi T, Kodama T, Isobe Y, Nakano D, Gokon N. Double-walled reactor tube with molten salt thermal storage for solar tubular reformers. Journal of Solar Energy Engineering-Transactions of the Asme. 2006;128:134-8.
[24] Gokon N, Nakano D, Inuta S, Kodama T. High-temperature carbonate/MgO composite materials as thermal storage media for double-walled solar reformer tubes. Solar Energy. 2008;82:1145-53.
[25] He YL, Tang SZ, Tao WQ, Li MJ, Wang FL. A general and rapid method for performance evaluation of enhanced heat transfer techniques. International Journal of Heat and Mass Transfer. 2019;145:118780.
[26] Zhang M, Hong Y, Ding S, Hu J, Fan Y, Voevodin AA, et al. Encapsulated nano-heat-sinks for thermal management of heterogeneous chemical reactions. Nanoscale. 2010;2:2790.
[27] Odunsi AO, O'Donovan TS, Reay DA. Dynamic Modeling of Fixed - Bed Fischer - Tropsch Reactors with Phase Change Material Diluents. Chemical Engineering & Technology. 2016;39:2066-76.
[28] Calverley EM, Witt PM, Sweeney JD. Reactor runaway due to statistically driven axial activity variations in graded catalyst beds. Chemical engineering science. 2012;80:393-401.
[29] Melis S, Varma A, Pereira CJ. Optimal distribution of catalyst for a case involving heterogeneous and homogeneous reactions. Chemical engineering science. 1997;52:165-9.
[30] Nie Y, Witt PM, Agarwal A, Biegler LT. Optimal active catalyst and inert distribution in catalytic packed bed reactors: ortho-xylene oxidation. Industrial & Engineering Chemistry Research. 2013;52:15311-20.
[31] Zheng ZJ, He Y, He YL, Wang K. Numerical optimization of catalyst configurations in a solar parabolic trough receiver-reactor with non-uniform heat flux. Solar Energy. 2015;122:113-25.
[32] Peppley BA, Amphlett JC, Kearns LM, Mann RF. Methanol–steam reforming on Cu/ZnO/Al 2 O 3 catalysts. Part 2. A comprehensive kinetic model. Applied Catalysis A General.

1999;179:31-49.
[33] Zheng ZJ, He Y, He YL, Wang K. Numerical optimization of catalyst configurations in a solar parabolic trough receiver–reactor with non-uniform heat flux. Solar Energy. 2015;122:113-25.
[34] Wang YJ, Liu QB, Lei J, Jin HG. A three-dimensional simulation of a parabolic trough solar collector system using molten salt as heat transfer fluid. Applied Thermal Engineering. 2014;70:462-76.
[35] He YL, Wang K, Qiu Y, Du BC, Liang Q, Du S. Review of the solar flux distribution in concentrated solar power: non-uniform features, challenges, and solutions. Applied Thermal Engineering. 2018;230:448-74.
[36] Gee R, Winston R. A Non-Imaging Secondary Reflector for Parabolic Trough Concentrators. Report to NREL, Duke Solar Energy, Raleigh, NC. 2001.
[37] Tsai CY, Lin PD. Optimized variable-focus-parabolic-trough reflector for solar thermal concentrator system. Solar Energy. 2012;86:1164-72.
[38] Wang K, He YL, Li P, Li MJ, Tao WQ. Multi-objective optimization of the solar absorptivity distribution inside a cavity solar receiver for solar power towers. Solar Energy. 2017;158:247-58.
[39] Qiu Y, He YL, Li PW, Du BC. A comprehensive model for analysis of real-time optical performance of a solar power tower with a multi-tube cavity receiver. Applied energy. 2017;185:589-603.
[40] Hsueh CY, Chu HS, Yan WM, Leu GC, Tsai JI. Three-dimensional analysis of a plate methanol steam micro-reformer and a methanol catalytic combustor with different flow channel designs. International Journal of Hydrogen Energy. 2011;36:13575-86.
[41] Ma Z, Yang WW, Li MJ, He YL. High efficient solar parabolic trough receiver reactors combined with phase change material for thermochemical reactions. Applied energy. 2018;230:769-83.
[42] Fridman E. Introduction to time-delay systems: Analysis and control: Springer; 2014.
[43] Tao WQ. Numerical heat transfer: Xi'an Jiaotong University Press, Xi'an; 2001.
[44] Sinnott RK. Chemical engineering design: Elsevier; 2014.

Performance Analysis and Optimization of Solar Thermochemical Reactor By Diluting Catalyst with Encapsulated Phase Change Material

Zhao Ma[a], Ming-Jia Li[a], Ya-Ling He[a,] *, K. Max Zhang[b]
a. Key Laboratory of Thermo-Fluid Science and Engineering of MOE, School of Energy and Power Engineering, Xi'an Jiaotong University, Xi'an, Shaanxi 710049, China
b. Sibley School of Mechanical and Aerospace Engineering, Cornell University, Ithaca, NY 14853, USA
*Corresponding author. Tel/Fax: +86-29-82665930
Email Address: yalinghe@mail.xjtu.edu.cn

Abstract: Solar thermochemical reactor, which can produce solar fuel at low cost, suffers discontinuous low-efficiency performance due to solar radiation fluctuation caused by cloud passage. To achieve highly efficient steady and dynamic performance of solar chemical reactor with less catalyst, in this study, catalytic activity is adjusted by diluting catalyst with encapsulated phase change material. At first, two-dimensional model of solar parabolic trough receiver reactors diluted with encapsulated phase change material is established and validated. Then, effect of catalytic activity on performance of reactor is discussed. Afterwards, one-dimensional model is derived from two-dimensional model to train Back Propagation neural network for quick and precise performance prediction of reactor. Finally, optimal catalytic distribution is obtained by genetic algorithm and Back Propagation neural network, and steady and unsteady performance of reactor between uniform and optimal catalytic distribution are compared. The results show that when catalytic activity decreases from 1.0 to 0.2, steady methanol conversion efficiency and production rate of H_2 are reduced by 8.4 % and 9.9 %, and reactor shows more stability under unsteady condition of solar radiation. One-dimensional model derived in present study is accurate enough and time-saving compared to two-dimensional model. And compared to reactor fully packed with catalyst, reactor with optimal catalytic distribution can achieve similar steady performance with 56 % less of catalyst, but shows better stability under the fluctuation of solar radiation.

Keywords: Solar thermochemical reactor; Solar radiation fluctuation; Phase change material; Catalytic activity's distribution; One-dimensional model

1. Introduction

Solar energy has increasingly been considered as a promising resource to energy crisis and global environmental problem[1]. Solar thermochemical reaction which can produce solar fuel, such as hydrogen or syngas, has attracted lots of attention due to its high efficiency, low cost and no pollution[2]. In solar thermochemical reaction, solar energy is concentrated to provide heat for chemical reactor and stored in solar fuels which can be further converted to electricity by fuel cell, gas turbine or internal combustion engine[3]. According to the operational temperature of chemical process, solar thermochemical reactions can be roughly sorted into two groups[4]: high temperature process and middle-and-low temperature process

Usually, high temperature solar thermochemical reactions operates above 800 ℃[4], such as H_2O and CO_2 splitting[5], methane reforming[6] and biomass gasification[7]. Chuayboonab and Abanades et al. [6] experimentally investigated the solar-driven methane and H_2O/CO_2 splitting in the temperature range of 950-1050 ℃ and the ceria cycling stability was also examined. They found that the highest solar-to-fuel conversion efficiency can reach 5.22 %. High operation temperature may lead to the decrease of system's thermal efficiency due to heat loss and optical loss, and also raise the technical difficulties for the design, fabricating and operation of such high temperature system[8], especially in large-scale commercial applications. Different from the high temperature chemical process, middle-and-low solar thermochemical reactions are often operated within 150-500 ℃[9], which shows great potential for real applications[4]. One of the promising middle-and-low thermochemical reactions for hydrogen is methanol steam reforming reactions because of its advantages that methanol can be producible from biomass, stays in liquid state for easy transportation and manipulation, and has high H/C ratio[10]. For example, Liu and Jin et al. [11] experimentally tested a 5-kW solar thermochemical reactor for methanol steam reforming heated between 150-300 ℃, and their experimental results showed that methanol conversion efficiency can be higher than 90%

and thermal-chemical conversion efficiency was in the range of 30-50 %, which is competitive with high-temperature solar thermochemical reactions.

However, weather transients cause a large challenge to the life span and safe operation of solar power plants[7, 12]. Suffered by solar radiation variation caused by cloud transients, the solar thermochemical reactor may endure the large temperature fluctuation, which can reduce the chemical conversion efficiency [12], deactivation of catalyst [13] and even lead to the sudden shut down of system [14]. Strategies have been explored to alleviate the adverse effect of solar radiation fluctuation, which can be divided into two types: active controlling strategy and passive thermal management. In active controlling strategy, the heliostats[15], flow rate of reactants[16] or additional equipment, such as electric heater[12], are often regulated to maintain the continuous high-performance operation of solar chemical reactor. For example, Rowe and Weimer et al.[12] employed feedback and predictive linear models controllers to regulate the solar-electric reactor for the production of syngas at 925 ℃ through the gasification of carbon under the cloud transient. They concluded that the controlling accuracy of model predictive control is more precise than that of feedback control. Meanwhile, it should be noted that the controlling performance of active controlling strategy is highly affected by the accuracy of solar radiation forecast, which is hard to be predicted precisely[17]. Moreover, the temperature detector may not be distributed uniformly or small sufficiently to detect micro-size hot or cold spot[18]. Also, controlling robustness and accuracy are difficult to be guaranteed in the control process of solar chemical reactor[12].

Another efficient way to maintain the continuous performance of solar chemical reactor is passive thermal management with phase change material (PCM), which can absorb/release large amount of latent heat at constant temperature during the phase transition. So far, PCM has widely applied in the thermal management of battery system to avoid the sudden uprising of temperature [19] and heat storage for the continuous operation of solar power plant[20]. Huang and Cheng et al[21] applied form-stable composite PCM in the thermal management of Li-ion battery pack experimentally. Their experimental results showed the battery temperature drops by 18 °C at 10 C discharge rate with flexible form-stable composite PCM, and Li-ion battery can safely work for an extended time within the upper temperature limit. Meanwhile, there are few studies on the application of PCM in the

thermal management of solar thermochemical reactors. Pattison and Baldea et al. [22] confined PCM in layer between the plates of reactor for auto-thermal methane-steam reforming reactor to avoid the unpredictable temperature excursion and that structure showed excellent disturbance rejection performance with hierarchical control structure. To mitigate the adverse effects of solar radiation fluctuations, Hatamachi and Gokon et al. [23, 24] applied PCM in the tubular solar chemical reactor for CO_2 reforming of methane (operated over 700 ℃), and bulk PCM is packed into shell side to form "double-wall" reactor. In their experiments, Na_2CO_3 is employed as phase change material and their experimental results demonstrated that the proposed "double-wall" reactor can realize stable operation when insulation fluctuates caused by cloud passage. Furthermore, to improve the heat transfer rate of PCM which is often limited by its low conductivity, in the study of Su et al. [25], instead of in bulk state, phase change material is encapsulated by silica, called encapsulated phase change material (EPCM)[26], and is mixed with catalyst to quench the local hot spots induced by non-uniform packing of catalyst and abrupt change of reaction rate. Their results showed that the EPCM can quenching the local hot point at initial stage and prevent thermal runaway. O. Odunsi et al. [18, 27] investigated temperature stability of Fischer Tropsch reactor in which catalyst is diluted with EPCM ($Sn@SiO_2$) homogeneously. Their results showed that better selectivity of long chain hydrocarbons (C_{5+}) to CH_4 can be achieved by mixing EPCM with catalyst. On the other hand, some researchers [28] try to improve the steady performance of exothermic reactor by adjust catalytic activity distribution through diluting catalyst by solid inertia particles. Lee and Varma et al.[29, 30] confirmed that the overall conversion of chemical reactor can be improved with proper distribution of catalytic material through experiments. Nie and Witt et al. [30] optimized the graded reactor activity profile for exothermic reaction to balance the heat generation by reaction with heat removal capacity and potentially improve chemical performance. Their results showed that compared with uniform distribution of catalytic activity, the 2-part optimized activity profile can improve the production rate by 26 %. It also should be noted that poor optimized activity profile can lead to thermal runaway even with catalyst dilution[28].

The literature review above indicates EPCM can well prevent the thermal runaway of exothermic reactor in chemical plants. However, the solar chemical reactor, which is different from the

exothermic reactor, is heated by solar energy and faces the fluctuation of solar radiation cause by weather transients. The potential of mix catalyst with EPCM to alleviate the adverse effect of solar radiation fluctuation is rarely investigated. On the other hand, as concluded from above discussion, that non-uniform distribution of catalytic activity has potential to improve the steady performance (such as such as conversion efficiency and production selectivity) of thermochemical reactor. However, in most of these studies, catalyst is diluted with solid particle, instead of EPCM. The steady and unsteady performances of solar thermochemical reactor with non-uniform distribution of catalytic activity, in which catalyst is diluted with EPCM, are still unknown. What's more, the optimal catalytic activity distribution of solar thermochemical reactor for methanol steam reforming needs to be further explored.

The overall objective of this paper is to alleviate the adverse effect of solar radiation fluctuation on solar thermochemical reactor with encapsulated phase change material. Specific objectives are to explore the steady and dynamic behavior of solar thermochemical reactor diluted with encapsulated phase change material, and then optimize the distribution of catalytic activity in solar reactor. To achieve these goals, in this paper, at first, a two-dimensional dynamic model is established and validated with experimental data. Then, thermal and chemical performance of solar thermochemical reactor uniformly diluted with EPCM under steady and unsteady conditions of solar radiation are comprehensively analyzed. Afterwards, to better utilize the catalyst in chemical reactor, effect of non-uniform distribution of catalytic activity on steady-state chemical performance of solar chemical reactor is analyzed. Furthermore, for the high-accuracy and time-saving prediction of the chemical performance for solar thermochemical reactor, a one-dimensional model which is simplified from two-dimensional model with reasonable assumptions is used to train the Back Propagation neural network. Finally, the catalytic activity distribution of catalyst in solar chemical reactor is optimized by genetic algorithm and Back Propagation neural network, and steady and dynamic behaviors of solar chemical reactor with uniform and optimal catalytic activity distribution are comprehensively compared.

2. Model

2.1 Physical model

Fig. 1 illustrates the structure of solar parabolic trough receiver reactor (SPTRR) filled with mixture bed of catalyst and encapsulated phase change material (EPCM). As shown in Fig. 1, the SPTRR consists of receiver tube, catalyst and EPCM. In present paper, the LS2 solar parabolic trough receiver [31] is employed to concentrate solar radiation and generate heat for the chemical reaction. The catalyst used for methanol steam reforming reaction is $Cu/ZnO/Al_2O_3$ [32] and is diluted with encapsulated phase change material (EPCM) of $Sn@SiO_2$[25], in which Sn is core material serving as phase change material and SiO_2 is the shell material with good inert[18]. Thermophysical properties of catalyst and EPCM are listed in Table 1. The outer and inner diameter of receiver tube are 0.07 and 0.066 m, respectively, and the length is 5 m[31]. The tube is made of stainless steel 310S. The density, specific heat and thermal conductivity of 310S respectively is 8 $g\cdot cm^{-3}$, 500 $J\cdot kg^{-1}\cdot K^{-1}$ and 14.2 $W\cdot m^{-1}\cdot K^{-1}$.

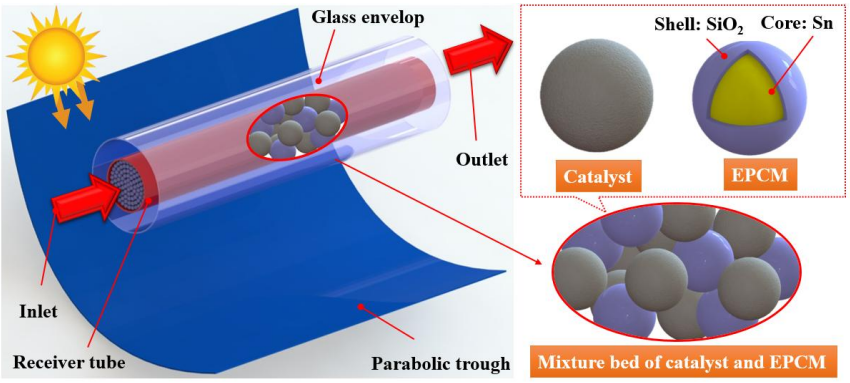

Fig. 1 Schematic diagrams of SPTRR diluted with EPCM

Table 1 Thermo-physical properties of catalyst and EPCM

Property	Value	Property	Value
Catalyst[33]		EPCM (Sn @ SiO_2)[18]	
ρ_{cat} /kg·m^{-3}	1300	ρ_{EPCM} /kg·m^{-3}	7184
$c_{p,cat}$ /J·kg^{-1} ·K^{-1}	542	$c_{p,EPCM}$ /J·kg^{-1}·K^{-1}	244
λ_{cat} /W·m^{-1}·K^{-1}	20	$\lambda_{p,EPCM}$ / W·m^{-1}·K^{-1}	67
ε_{cat} and ε_{EPCM}	0.4	T_m/ K	505
		ΔT_m /K	2
		L_{EPCM}/ J·kg^{-1}	60500

In chemical reactor, reactants (methanol and steam both in vapor state) flow through reactor tube,

heated by solar radiation, undergoes chemical reaction on the surface of catalyst and are converted to hydrogen, carbon dioxide and carbon monoxide.

The concentrated solar radiation is non-uniformly distributed on the surface of reactor tube, but its effect on solar chemical reactor is negligible, which is indicated in ref. [34]. Meanwhile, some methods can be employed to largely improve the uniformity of solar radiation on reactor tube, such as[35] adding secondary reflector[36], variable focus parabolic trough[37], distribution optimization of solar absorption in receiver[38] and optimization of aiming strategy[39]. Herein, it is reasonable to assume that solar radiation is uniformly distributed on the surface of solar chemical reactor tube. Besides, some other assumptions are made to establish computational model as follows.

(1) The inlet mass flow rate and temperature of reactants (methanol and steam) are constant.

(2) The reactants (methanol and steam) and reaction productions (hydrogen, carbon dioxide and carbon monoxide) can be treated as ideal gas[33].

(3) Catalyst and EPCM are in same size[30], and the mixture of catalyst and EPCM bed is treated as isotropic porous media.

(4) The fluid phase and solid phase in chemical reactor are in local thermal equilibrium[18].

Using catalytic activity σ, the volume ratio f_{EPCM} of EPCM to mixture can be calculated[27] by:

$$f_{\mathrm{EPCM}} = 1-\sigma \tag{1}$$

where, σ is the catalyst activity.

Thus, thermo-physical properties of the mixture of catalyst EPCM can be calculated by following Equations [18, 27]:

$$\rho_{\mathrm{mix}} = \sigma\rho_{\mathrm{cat}} + \left(1-\sigma\right)\rho_{\mathrm{EPCM}} \tag{2}$$

$$\theta_{\mathrm{mix}} = \frac{\rho_{\mathrm{cat}}}{\rho_{\mathrm{cat}}+\rho_{\mathrm{EPCM}}}\theta_{\mathrm{cat}} + \frac{\rho_{\mathrm{EPCM}}}{\rho_{\mathrm{cat}}+\rho_{\mathrm{EPCM}}}\theta_{\mathrm{EPCM}} \tag{3}$$

where θ represents the thermal conductivity and specific heat of the mixture bed.

2.2 Governing equation

The computational domain contains two parts: mixture bed of catalyst and EPCM and reactor tube, which is illustrated in Fig. 2. Because SPTRR is axial symmetry, two-dimensional model is

employed. Governing equations of each part are displayed as follows.

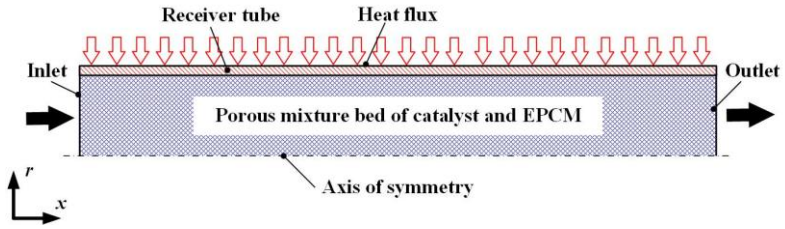

Fig. 2 Computational domain of SPTRR in which the catalyst is mixed with EPCM

2.2.1 The porous mixture bed of catalyst and EPCM:

Governing equations of the porous mixture bed include continuity equation, momentum equation, specie equation and energy conversation equation, which can be expressed as follows.

The continuity equation:

$$\frac{\partial\left(\varepsilon_{\mathrm{mix}}\rho\right)}{\partial t}+\nabla\cdot\left(\varepsilon_{\mathrm{mix}}\rho\vec{u}\right)=0 \tag{4}$$

where $\varepsilon_{\mathrm{mix}}$ represents the porosity of the porous mixture bed.

The momentum equation:

$$\frac{\partial\left(\varepsilon_{\mathrm{mix}}\rho\vec{u}\right)}{\partial t}+\nabla\cdot\left(\varepsilon_{\mathrm{mix}}\rho\vec{u}\vec{u}\right)=-\varepsilon_{\mathrm{mix}}\nabla p+\nabla\cdot\left[\varepsilon_{\mathrm{mix}}\left(\mu_{\mathrm{t}}+\mu\right)\left(\frac{\partial u_i}{\partial x_j}+\frac{\partial u_j}{\partial x_i}\right)-\frac{2}{3}\varepsilon_{\mathrm{mix}}\left(\mu_{\mathrm{t}}+\mu\right)\delta_{ij}\nabla\cdot\vec{u}\right]+\vec{S}_i \tag{5}$$

where μ_{t} and μ are, respectively, the turbulent and dynamic viscosity of flow fluid, $\vec{S}_i$ represents momentum source term. The dynamic viscosity μ can be obtained in Ref. [40]. The source term of momentum equation can be can be found in Ref. [33].

The species conservation equation for each specie *i* can be depicted as:

$$\frac{\partial\left(\rho m_i\right)}{\partial t}+\nabla\cdot\left(\rho\vec{u}m_i\right)=\nabla\cdot\left[\left(\rho D_{m,i}+\frac{\mu_{\mathrm{t}}}{Sc_{\mathrm{t}}}\right)\nabla m_i\right]+Y_i \tag{6}$$

where m_i and $D_{m,i}$, respectively, are mass fraction and mass diffusion coefficient of specie *i*, Sc_{t} represents Schmidt number, which is set to be 0.7[31] in present study. Y_i is the source term for chemical reaction of specie *i* and its expression can be found in our prior work[41].

Reactions occurring in the porous mixture bed of catalyst and EPCM bed mainly contains 3 different chemical processes: methanol steam reforming reaction (MSR), methanol decomposition reaction (MDR), and water–gas shift reaction (WSR), which are expressed as follows:

$$CH_3OH + H_2O \rightleftharpoons CO_2 + 3H_2 \tag{7}$$

$$CH_3OH \rightleftharpoons CO + 2H_2 \tag{8}$$

$$CO + H_2O \rightleftharpoons CO_2 + H_2 \tag{9}$$

The comprehensive chemical kinetic model of methanol steam reforming model proposed by Peppley et al[32] is employed in this paper, which are shown in Eq. (10) - (12).

$$R_R = \frac{\sigma k_R K_{CH3O_{(1)}} \frac{p_{CH3OH}}{p_{H_2}^{1/2}} \left(1 - \frac{p_{H_2}^3 p_{CO_2}}{K_R p_{CH_3OH} p_{H_2O}}\right) C_{S1} C_{S1a} S_g}{\left(1 + K_{CH_3O_{(1)}} \frac{p_{CH_3OH}}{p_{H2}^{1/2}} + K_{HCOO} p_{CO_2} p_{H_2}^{1/2} + K_{OH_{(1)}} \frac{p_{H_2O}}{p_{H_2}^{1/2}}\right)\left(1 + K_{H_{(1)}}^{1/2} p_{H_2}^{1/2}\right)} \tag{10}$$

$$R_D = \frac{\sigma k_D K_{CH3O_{(2)}} \frac{p_{CH3OH}}{p_{H_2}^{1/2}} \left(1 - \frac{p_{H_2}^2 p_{CO}}{K_D p_{CH_3OH}}\right) C_{S2} C_{S2a} S_g}{\left(1 + K_{CH_3O_{(2)}} \frac{p_{CH_3OH}}{p_{H2}^{1/2}} + K_{OH_{(2)}} \frac{p_{H_2O}}{p_{H_2}^{1/2}}\right)\left(1 + K_{H_{(2)}}^{1/2} p_{H_2}^{1/2}\right)} \tag{11}$$

$$R_W = \frac{\sigma k_W K_{OH_{(1)}} \frac{p_{CO} p_{CH3OH}}{p_{H_2}^{1/2}} \left(1 - \frac{p_{H_2} p_{CO_2}}{K_W p_{CO} p_{H_2O}}\right) C_{S1}^2 S_g}{\left(1 + K_{CH_3O_{(1)}} \frac{p_{CH_3OH}}{p_{H2}^{1/2}} + K_{HCOO} p_{CO_2} p_{H_2}^{1/2} + K_{OH_{(1)}} \frac{p_{H_2O}}{p_{H_2}^{1/2}}\right)^2} \tag{12}$$

where σ represents the catalytic activity of the porous mixture ranging from 0 to 1, R_R, R_D and R_W are the reaction rate of MSR, MDR and WSR, respectively, p_i represents the partial pressure of specie i, C_{S1} and C_{S2}, respectively, are the concentration of active site S1 and S2 on the catalyst surface, S_g presents the surface area of catalyst. These detailed parameters can be found in our prior work[41].

The molar consumption rate of CH_3OH R_{CH_3OH} (in unit of $mol \cdot m^{-3} \cdot s^{-1}$) can be obtained by Eq. (13).

$$R_{CH_3OH} = -\left(R_R + R_D\right) \tag{13}$$

The energy conservative equation in the mixture bed of catalyst EPCM, based on the local thermal equilibrium, is given by:

$$\frac{\partial\left[\varepsilon_{mix}\rho_f c_{p,f} T + \left(1-\varepsilon_{mix}\right)\rho_{mix} c_{p,mix} T\right]}{\partial t} + \nabla \cdot \left(\rho_f c_{p,f} \vec{u} T\right) = \nabla \cdot \left(\lambda_{eff} \nabla T\right) + S_t \tag{14}$$

where the energy source term S_t can be found in our prior work[41].

In present study, the "effective heat capacity method" is employed to calculate the specific heat of EPCM during phase transition[18], which is shown in Eq. (15)

$$c_{p,\mathrm{EPCM,eff}} = \begin{cases} c_{p,\mathrm{EPCM}}, & T < T_{\mathrm{m}} - \dfrac{\Delta T}{2} \\ c_{p,\mathrm{EPCM}} + \dfrac{L_{\mathrm{EPCM}}}{\Delta T}, & T_{\mathrm{m}} - \dfrac{\Delta T}{2} \le T < T_{\mathrm{m}} + \dfrac{\Delta T}{2} \\ c_{p,\mathrm{EPCM}}, & T \ge T_{\mathrm{m}} + \dfrac{\Delta T}{2} \end{cases} \tag{15}$$

where ΔT is set to 2 K in this study[18].

2.2.2 The receiver tube:

The energy conversion equation describing heat conduction in the reactor tube is given by：

$$\frac{\partial\left(\rho c_p T\right)_{\mathrm{tube}}}{\partial t} = \nabla\cdot\left(\lambda_{\mathrm{tube}}\nabla T\right) \tag{16}$$

where λ_{tube} is the thermal conductivity of reactor tube.

2.3 Boundary condition

As illustrated in the Fig. 2, the boundary conditions of the simulation domain can be shown as follows:

(1) For porous mixture of catalyst and EPCM, the inlet and outlet boundaries are expressed as:

Inlet boundary: molar of molar ratio of H_2O/CH_3OH is set to 1.1, and temperature and flow velocity are constant, namely $u=u_{\mathrm{in}}$, $T=T_{\mathrm{in}}$=423.15 K, $M_{\mathrm{H_2O}}/M_{\mathrm{CH_3OH}}$=1.1.

Outlet boundary: the outlet pressure keeps constant, namely $p=p_{\mathrm{out}}$=101325 Pa.

(2) For the reactor tube region, the end surfaces of tube are constrained as adiabatic walls: $\partial T/\partial x = 0$.

(3) The boundary for axis of symmetry is expressed as: $\dfrac{\partial\vec{u}}{\partial r} = \dfrac{\partial T}{\partial r} = 0$

(4) The interface of tube region and mixture region is defined as the coupled fluid–solid interface, namely, $\vec{u} = 0$, $T_{\mathrm{cat}} = T_{\mathrm{tube}}$.

(5) In this study, the average local concentration ratio of solar collector is set to 20[31], and the direct normal irradiance (DNI) is assumed to be 600 $W \cdot m^{-2}$, herein, thus the heat flux on the surface of reactor tube is equal to 12000 $W \cdot m^{-2}$.

2.4 Definition of performance indicator

In present paper, the steady and unsteady performance of SPTRR are both investigated, thus some performance indicators are defined.

For steady condition of solar radiation, the performance of SPTRR is evaluated by methanol conversion efficiency η_c, which is expressed as:

$$\eta_c = \frac{\dot{m}_{CH_3OH,in} - \dot{m}_{CH_3OH,out}}{\dot{m}_{CH_3OH,in}} \tag{17}$$

where $\dot{m}_{CH_3OH,in}$ and $\dot{m}_{CH_3OH,out}$, respectively, represent the inlet and outlet mass flow rate of chemical reactor.

Due the weather transients, the solar radiation variation with time can be roughly divided into two different kinds: single-step fluctuation and successive fluctuation. Fig. 3 illustrates the illustration of two different typical solar radiation fluctuations. Thus, in present paper, for unsteady condition of solar radiation, Delay response time $\Delta t_{50,\eta_c}$ [42] and relatively vibrating amplitude of methanol conversion efficiency γ_{η_c} are adopted for the dynamic performance evaluation of SPRR under the single-step and successive fluctuations of solar radiation respectively.

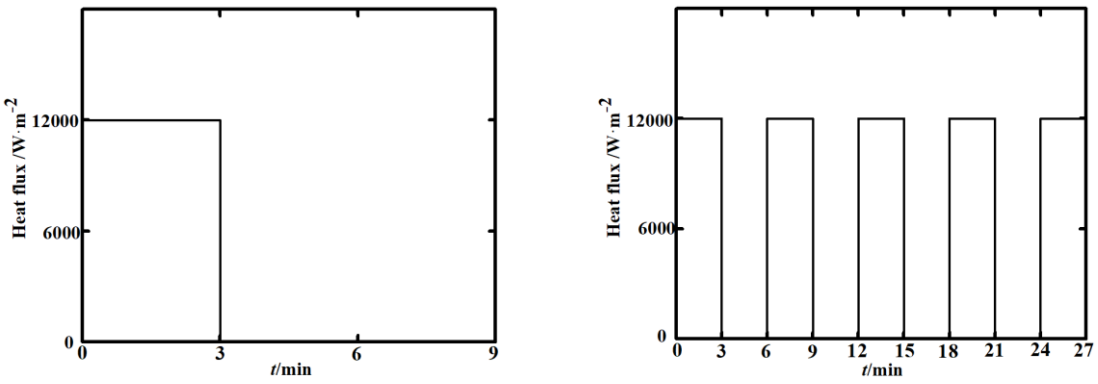

(a) Single step fluctuation (b) Successive step fluctuation

Fig. 3 Illustration of two different typical solar radiation fluctuations

Delay response time $\Delta t_{50,\eta_c}$ [42] is defined as the time during which the methanol conversion

efficiency changes by 50 % of $\Delta\eta_{c,total}$, which is illustrated in Fig. 4 And $\Delta\eta_{c,total}$ is total change of methanol conversion efficiency due to the step fluctuation of solar radiation. $\Delta t_{50,\eta_c}$ can reflect the ability of solar chemical reactor to delay the adverse effect of single fluctuation of solar radiation.

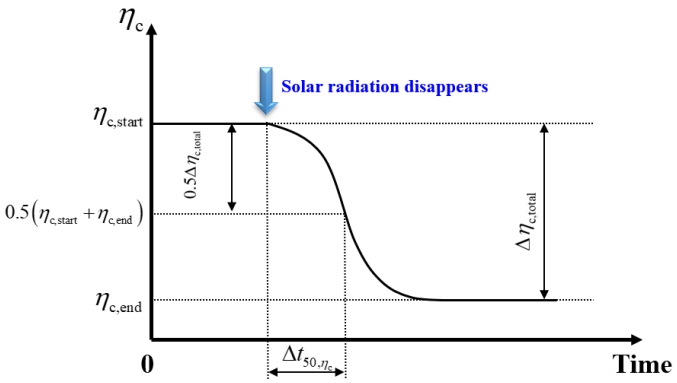

Fig. 4 Graphic illustration of delay response time $\Delta t_{50,\eta_c}$

The relatively vibrating amplitude of methanol conversion efficiency γ_{η_c} is defined as ratio of the vibrating amplitude value and time-average value of methanol conversion efficiency after solar chemical reactor reaches the repeatable state under successive fluctuations of solar radiation, and can be expressed as:

$$\gamma_{\eta_c}=\frac{\left(\eta_{c,max}-\eta_{c,min}\right)/2}{\eta_{c,ave}} \tag{18}$$

where $\eta_{c,max}$, $\eta_{c,min}$ and $\eta_{c,ave}$ are, respectively, the maximum, minimum and time-average value of methanol conversion efficiency during one repeatable cycle. And γ_{η_c} can reveal the stability of solar chemical reactor under successive fluctuations of solar radiation.

2.5 Numerical method and model validation

The governing equations described above are solved by Finite Volume Method, and the convective terms in momentum, species and energy conversion equations are discretized by second upwind scheme. SIMPLE algorithm[43] is employed to couple the velocity and pressure. Computational Fluid Dynamics (CFD) software FLUENT is used to solve the governing equations. The methanol conversion efficiency and outlet temperature calculated by four different grid systems

(i.e., 2500(x) ×18(r), 3333×23, 5000×35, 10000×70) are compared to exam the gird independence and the results are shown in Fig. 5 (a). As can be seen, the difference of predicted results including methanol conversion efficiency and outlet temperature between the grid systems of 5000(x)×35(r) and 10000(x)×70(r) is negligible, thus the gird system of 5000(x)×35(r) is adequate for predicting the thermal and chemical performance of SPTRR and adopted in following simulations. As for the independence test of time step, results calculated by four different time steps ranging from 0.5s to 5s are compared, which are illustrated in Fig. 5 (b). It can be seen that, the difference of methanol conversion efficiency variation curve with time predicted by 1s and 2s are quite close, and the time step of 2s is used in simulations for its sufficient accuracy and acceptable computational cost.

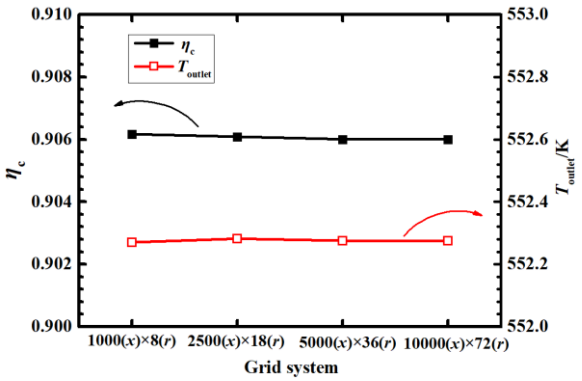

(a) Independence test of grid system

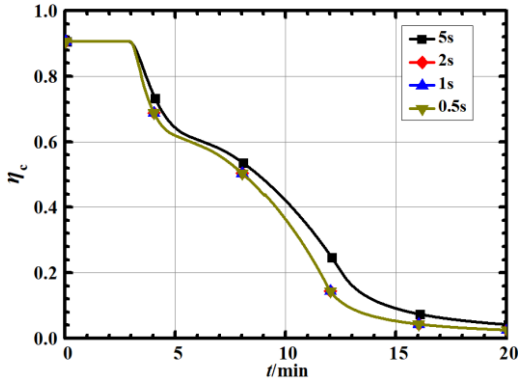

(b) Time-step independence test(Variation of methanol conversion efficiency with time)

Fig. 5 Grid and time-step independence test

The validation result of model can be found in our previous paper, which shows the model established is accurate enough to predict the performance of SPTRR.

3. Results and discussion

3.1 Thermal and chemical performance of SPTRR with uniform distribution of catalytic activity

In this section, the thermal and chemical performance of SPTRR with different catalytic activities under steady and unsteady condition of solar radiation are analyzed. In simulations, the inlet mass flow rate of reactants is equal to 0.01 kg·s^{-1}. The heat flux on the outer surface of reactor is set to 12000 W·m^{-2} for steady condition of solar radiation and varies with time for unsteady condition of solar radiation as illustrate in Fig. 3.

3.1.1 Thermal and chemical performance of SPTRR under steady condition of solar radiation

Fig. 6 (a) and (b) present the cross-sectional averaged temperature and molar consumption rate of CH_3OH variation along the flow direction for different catalytic activities, respectively. As can be seen from Fig. 6 (a), when x is smaller than 0.5 m, the cross-sectional averaged temperature of flow fluids increases rapidly along the flow direction due to the heat flux on the surface of reactor tube. Then, the rising rate of temperature is slower and keeps constant because of the high reaction rate of endothermic methanol steam reforming reaction, as is shown in Fig. 6 (b). And when x is larger than 4 m, the increasing rate of temperature is elevated again which is leaded by the decreasing of reactants' concentration and reduced reaction rate. For SPTRR with different catalytic activities, as catalytic activity decreases, the temperature at same position of x is improved and the highest consumption rate of CH_3OH in SPTRR is lower, indicating that more solar energy is converted to the sensible heat of reactants and productions instead of chemical energy.

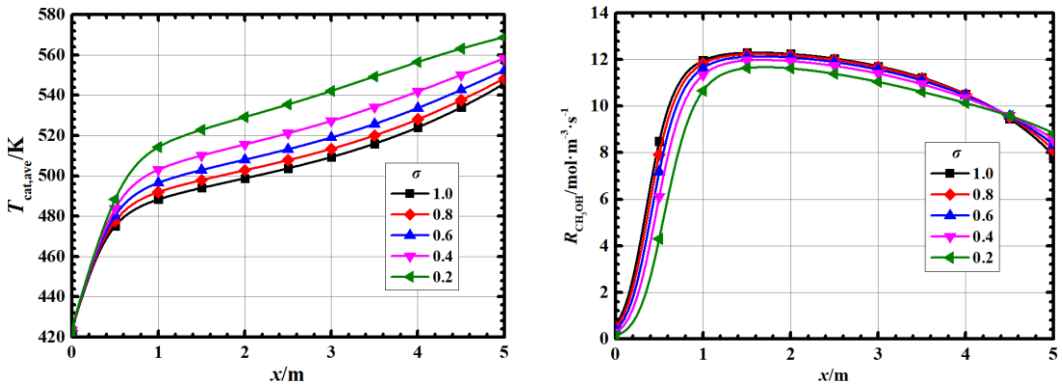

(a) Average temperature (b) Molar consumption rate of CH_3OH

Fig. 6 Cross-sectional averaged temperature and molar consumption rate of CH_3OH variation along the fluid direction for different catalytic activities

To avoid the sintering failure of catalyst and keep the safe operation of SPTRR, the reactor should be operating below the upper temperature limit of catalyst $Cu/ZnO/Al_2O_3$ (573 K). Fig. 7 presents thermal and chemical performance of SPTRR with different catalytic activities under steady condition. As can be seen from this figure that, as the catalytic activity decreases from 1.0 to 0.2, the maximum temperature of catalyst increases from 552 to 573 K, which is within the allowable temperature range of $Cu/ZnO/Al_2O_3$ catalyst for safe operation[32]. As for the chemical performance, it can be seen that, with the decrease of catalytic activity, the methanol conversion efficiency and

production rate of H_2 are both gradually reduced due to the decline of reaction rate, while production rate of CO is improved a lot due to the higher reaction rate of methanol decomposition reaction which produces CO. When catalytic activity decreases from 1.0 to 0.2, methanol conversion efficiency and $\dot{m}_{H_2}$ are reduced by 8.4 % and 9.9 % respectively, while $\dot{m}_{CO}$ rises by 121.3 %

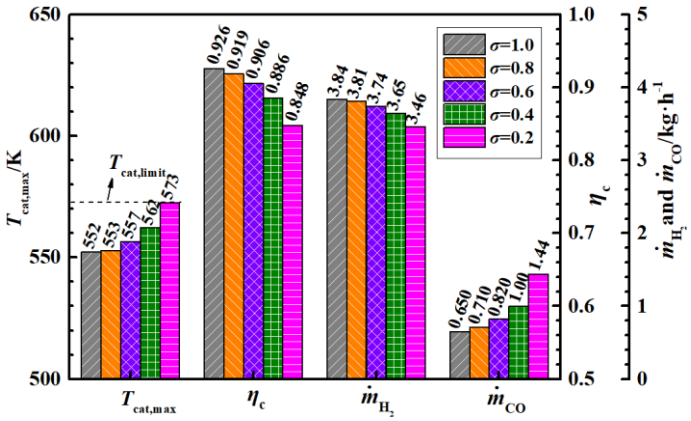

Fig. 7 Thermal and chemical performance of SPTRR with different catalytic activities under steady condition

3.1.2 Thermal and chemical performance SPTRR with under unsteady condition of solar radiation

In this section, the dynamic behavior of SPTRR with different catalytic activities are analyzed. There are two different types of solar radiation fluctuations: single step fluctuation and successive step fluctuation. In simulations, the nominal heat flux on the surface of reactor is 12000 W·m^{-2}. For the singe step fluctuation of solar radiation, the heat flux on the surface of reactor tube drops from 12000 W·m^{-2} to zero after t is larger than 3 min, as is shown Fig. 3 (a). For the successive step fluctuation of solar radiation, the heat flux switches between 12000 W·m^{-2} and zero for every 3 mins, which is illustrated in Fig. 3 (b).

(1) Single-step fluctuation of solar radiation

Fig. 8 (a) and (b) show $T_{cat,ave}$ and η_c variation with time of SPTRR with different catalytic activities under single step fluctuation of solar radiation, respectively. Clearly, when σ=1.0 (catalyst is not diluted with EPCM), after solar radiation disappears at t=3min, $T_{cat,ave}$ and η_c both decrease rapidly at first due to the short of heat supply, and then gradually reaches a stable value. While for σ

lower than 1.0 (catalyst is diluted with EPCM), compared with σ=1, the decreasing process of $T_{\mathrm{cat,ave}}$ and η_{c} after the disappearance of solar radiation is slower, and there exists a turning point in their decreasing processes due to the large latent heat released by EPCM. It can also be found that as σ declines, the turning point of $T_{\mathrm{cat,ave}}$ is higher, while the turning point of η_{c} decreases gradually. This phenomena can be explained by the fact that when the catalytic activity decreases, which means catalyst is diluted by more EPCM, the reaction rate at the same temperature decreases thus the turning point of methanol conversion efficiency declines. Meanwhile, with lower catalytic activity and higher filling proportion of EPCM in SPTRR, more latent heat can be released for endothermic chemical reactions (MSR and MD) in the temperature decreasing process, and temperature decreases slower, thus chemical reactions keeps lower methanol conversion efficiency at higher temperature for longer time. When the catalytic activity σ is diluted from 0.8 to 0.2, the turning value of η_{c} decreases from 0.72 to 0.38 greatly, which is reduced by 47.2 %.

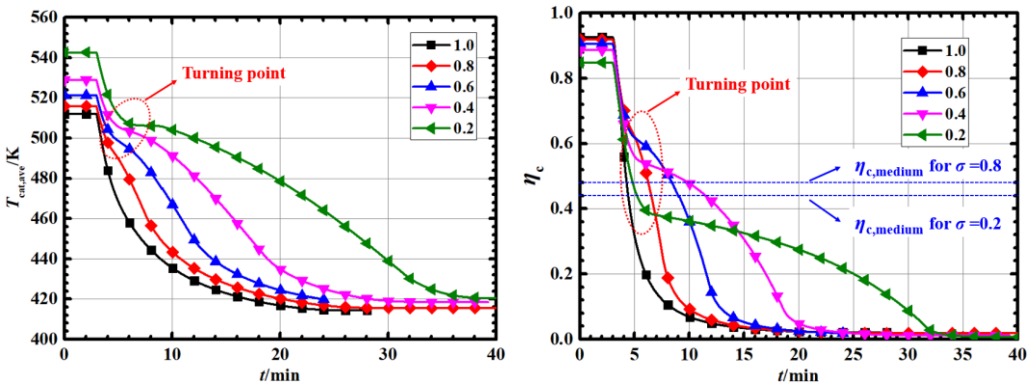

(a) Average temperature of catalyst (b) Methanol conversion efficiency

Fig. 8 $T_{\mathrm{cat,ave}}$ and η_{c} variation with time of SPTRR with different catalytic activities under single step fluctuation of solar radiation

Fig. 9 shows influence of catalytic activity on delay response time of SPTRR under step fluctuation of solar radiation. As can be seen in this figure, with the decreasing of σ from 1.0 to 0.2, $\Delta t_{50,\eta_{\mathrm{c}}}$ increases at first and reaches the maximum value of 8.2 mins at σ=0.4, then declines. This phenomena is caused by the reason that as σ decreases from 1.0 to 0.4, the content of EPCM in SPTRR becomes larger and the decreasing rate of methanol conversion efficiency is slower. However,

when σ is equal to 0.2, the turning point of methanol conversion efficiency in the decreasing process is lower than $\eta_{c,medium}$ (0.428, as shown in Fig. 8 (b)), therefore, the increasing of thermal inertia caused by EPCM makes little contribution to improvement of delay response time $\Delta t_{50,\eta_c}$. Compared with SPTRR fully packed with catalyst (σ=1), when σ is equal to 0.4, $\Delta t_{50,\eta_c}$ of SPTRR under step fluctuation of solar radiation is prolonged by 845 %, which means longer response time and can leave longer time for control system to make response.

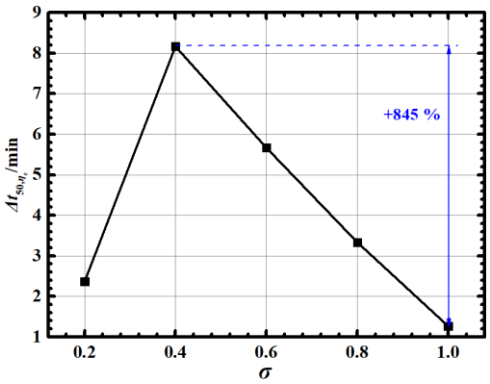

Fig. 9 Influence of catalytic activity on $\Delta t_{50,\eta_c}$ of SPTRR under step fluctuation of solar radiation

(2) Successive fluctuations of solar radiation

When the methanol conversion efficiency is relatively low (less than 0.3), the following process of separation and purification after reaction, such as pressure swing adsorption[11], will consumes lots of energy, which damages the economy of solar thermochemical reaction system. Similar with ref[13], in present paper the lowest limit of methanol conversion efficiency is set to 0.3.

Fig. 10 (a) shows the η_c variation with time of SPTRR for different catalytic activities under successive fluctuations of solar radiation. From Fig. 8 (a), it can be seen that η_c of SPTRR vibrates with the fluctuation of solar radiation, and finally can reach a repeatable state. Clearly, compared with SPTRR fully packed with EPCM (σ= 1.0), when catalyst is diluted with EPCM (σ= 0.2 and 0.6), the vibration amplitude of η_c is smaller, and the lowest value of η_c in the vibrating process is also improved after SPTRR reaches a repeatable state. For example, compared with σ= 1.0, when σ is diluted by EPCM to 0.2, the lowest value of η_c in a repeatable cycle is improved from 0.192 to 0.328, which is higher than lowest limit of methanol conversion efficiency (0.3) and can avoid the

sudden shut down of chemical reaction system. Fig. 8 (b) illustrates average value and relative vibrating amplitude of η_c after SPTRR reach repeatable state. Clearly, when catalyst is diluted by EPCM and σ decreases from 1.0 to 0.2, $\eta_{c,ave}$ increases at first and reaches maximum of 0.459 at σ=0.4, and then decreases due to its low catalytic activity, meanwhile, γ_{η_c} declines rapidly initially and reaches the lowest value of 0.223 at σ=0.4 due to its large thermal inertia. Compared with σ=1.0, the average value and relatively vibrating amplitude of methanol conversion efficiency in SPTRR with σ=0.4 are, respectively, prompted by 11.7 % and reduced by 69.8 %, which shows better stability of SPTRR under successive step fluctuation of solar radiation.

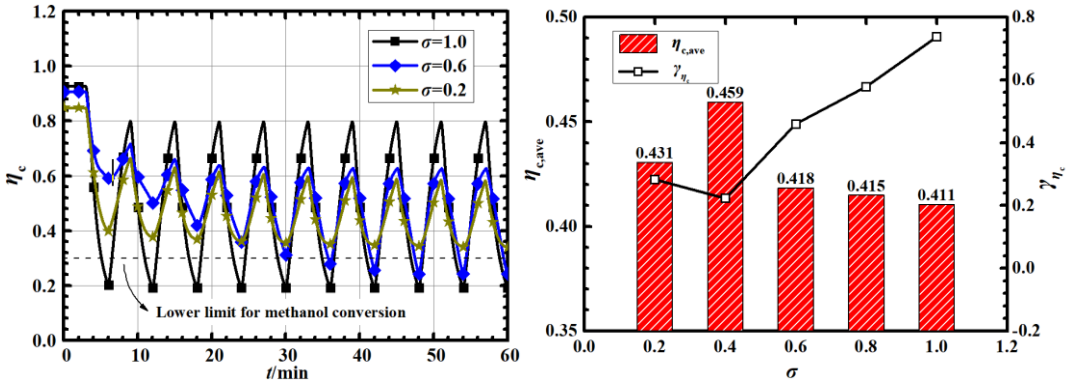

(a) Methanol conversion efficiency

(b) $\eta_{c,ave}$ and γ_{η_c}

Fig. 10 Variation and relatively vibrating amplitude of η_c in SPTRR with different catalytic activities under successive fluctuations of solar radiation

3.2 Chemical performance of SPTRR with non-uniform distribution of catalytic activity

As mentioned above, when catalyst is diluted with large amount of EPCM, the unsteady performance of STPRR can be greatly improved. However, due to the decrease of catalytic activity, the chemical performance of SPTRR under steady solar radiation, such methanol conversion efficiency, declines. To achieve high steady performance and stable dynamic behavior at the same time, non-uniform distribution of catalytic activity is applied in SPTRR. In this section, the chemical performance of SPTRR with 2-part distribution of catalytic activity, which is shown in Fig. 11, is analyzed. σ_1 and σ_2 are the catalytic activity at the front and end part of reactor respectively.

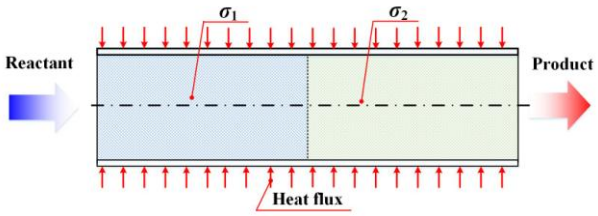

Fig. 11 Illustration of 2-part SPTRR with different catalytic activities

Fig. 12 depicts the methanol conversion efficiency of SPTRR with 2-part distribution of catalytic activity under steady condition. It is found that when the front-part catalytic activity σ_1 is constant, with the increasing of end-part catalytic activity σ_2, the methanol conversion efficiency of SPTRR is improved gradually. Correspondingly, it should be noted that, on the condition that σ_2 is constant, the effect of σ_1 on methanol conversion efficiency of SPTRR highly depends on the value of σ_2. That is, when σ_2 keeps equal to 0, improvement of σ_1 can lead to the uprising of η_c. However, when σ_2 keeps larger or equal to 0.2, the variation of σ_1 has negligible effect on η_c of SPTRR. For example, when σ_2 is equal to 1.0, as σ_1 varies between in the range of 0.2 to 1.0, η_c of SPTRR changes very little from 0.924 to 0.926. Thus, it can be concluded that the effect of catalytic activity on η_c depends on the catalyst position in SPTRR. This phenomena is caused by the fact the catalyst temperature increases along with the flow direction, and with same catalytic activity, based on the Arrhenius equation[44], the reaction rate at the end part is much larger than that at the front part, thus the effect of catalytic activity's variation at the end part (σ_2) on methanol conversion efficiency is more prominent than that at front part. Therefore, in order to achieve efficient steady and unsteady performance at the same time, it is be a feasible way to keep high methanol conversion efficiency, low total catalytic activity (i.e. large amount of EPCM) and high thermal inertia simultaneously by properly adjusting the distribution of catalytic activity. For example, by adjusting the catalytic activity distribution form all catalyst ($\sigma_1=\sigma_2=1.0$) to distribution of $\sigma_1=0.2$ and $\sigma_2=1.0$, the methanol conversion efficiency keeps high level (drops by less than 0.4%) with 40% decline of average catalytic activity, indicating much less usage of catalyst and huge amount of EPCM with large thermal

inertia.

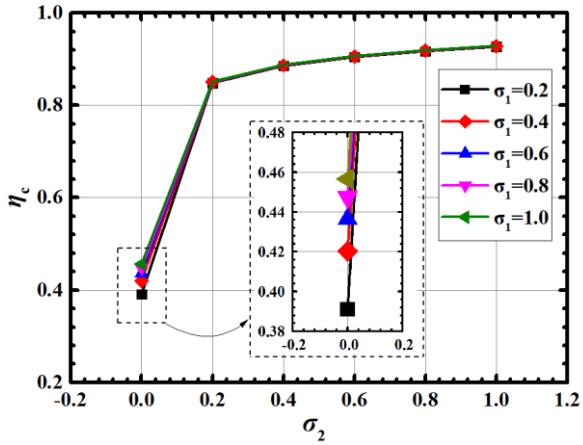

Fig. 12 Methanol conversion efficiency of SPTRR with 2-part distribution of catalytic activity

3.3 Distribution optimization of catalytic activity in SPTRR under steady condition of solar radiation

To achieve the efficient steady and unsteady performance of SPRR simultaneously, namely keeps high methanol conversion efficiency, high content of EPCM and low average catalytic activity at the same time, SPTRR is separated into 3 parts along the flow direction equally, and the catalytic activity of each part is optimized. Firstly, based on some reasonable assumptions, the two-dimensional model is simplified to one-dimensional model, which is validated by the results predicted by two-dimensional model. Then, the Back Propagation (BP) neural network is trained and validated with dataset calculated by 1-dimensional model for quick prediction of methanol conversion efficiency. Finally, using the trained BP neural network, the distribution of catalytic activity in SPTRR is optimized by Genetic Algorithm (GA), and chemical performance of SPTRR with optimized distribution of catalytic activity and fully packed with catalyst (σ=1) are compared.

3.3.1 Simplification of two-dimensional governing equation

To reduce the computational cost and keep high calculation precision at the same time, some assumptions are made to derive the 1-dimensional model from 2-dimensional model[30]:

(1) The concentration gradient of reactants and productions along the radial direction are negligible ($\partial m_i/\partial r$ = 0), because of the rapid diffusion of reactant and production along the radial

direction, and small radial concentration difference.

(2) The radial temperature gradient is considered in simulation because large amount of heat is absorb by the surface of reactor tube.

(3) The temperature distribution along radial direction can be approximated to parabolic curve. In present study, temperature profile along the radial direction is depicted as:

$$T(x,r)=\left[1+a\left(\frac{r}{R_{\text{reactor}}}\right)^2\right]T(x,0) \tag{19}$$

where, x and r represent the axial and radial coordinates, respectively, a is the coefficient related with the distribution profile of temperature, R_{reactor} represents the radius of chemical reactor.

To determine the temperature profile coefficient a of solar chemical reactor for methanol steam reforming reaction, radial temperature distributions of SPTRR are calculated by two-dimensional model, and the results are used to fit the temperature profile coefficient a by least square method. The obtained temperature profile coefficients for different catalytic activities which are shown in Table 2

Table 2 Distribution coefficient of radial temperature profile for different catalytic activities

σ	1.0	0.8	0.6	0.4	0.2	0
$a/\times10^{-3}$	28.196	11.328	9.1992	8.511	7.715	19.790

The average temperature of cross-sectional area can be derived by Eq. (20)

$$\overline{T}(x)=\frac{\int_0^{R_{\text{reactor}}}\left[1+a\left(\frac{r}{R_{\text{reactor}}}\right)^2\right]T(x,0)\cdot 2\pi r\mathrm{d}r}{\pi R_{\text{reactor}}^2}=\left(1+\frac{a}{2}\right)T(x,0) \tag{20}$$

Thus, the local temperature of SPTRR can be expressed with $\overline{T}(x)$, which can be derived by Eq. (21) using

$$T(x,r)=\frac{\left[1+a\left(\frac{r}{R_{\text{reactor}}}\right)^2\right]}{1+\frac{a}{2}}\overline{T}(x) \tag{21}$$

The one-dimensional models of species equation and energy conversation equation can be obtained by integrating Eq. (6)and Eq. (14) along the cross-sectional area of SPTRR, which are expressed in Eq. (23) and Eq. (22).

$$\frac{\partial(\rho m_i)}{\partial t}+\nabla\cdot(\rho u m_i)=\nabla\cdot\left[\left(\rho D_{m,i}+\frac{\mu_t}{Sc_t}\right)\nabla m_i\right]+F\cdot\sigma M_{w,i}\sum_{r=1}^{N_R}\hat{R}_{i,r}\left(\overline{T}\right) \tag{22}$$

$$\frac{\partial\left(\rho c_p\overline{T}\right)}{\partial t}+\nabla\cdot\left(\rho c_p u\overline{T}\right)=\lambda_{\text{eff}}\frac{\partial^2\left(\overline{T}\right)}{\partial x^2}+S_{\text{solar}}+F\cdot St\left(\overline{T}\right) \tag{23}$$

where the energy source term S_{solar} is caused by solar radiation and defined in Eq. (24), F is the correction coefficient for cross-sectional average reaction rate.

$$S_{\text{solar}}=\frac{2\pi R_{\text{reactor}}\cdot q}{\pi R_{\text{reactor}}^2} \tag{24}$$

According to Arrhenius Equation[44], the relation between reaction rate $R(T)$ and temperature can be expressed as[27]:

$$R(T)=R\left(\overline{T}\right)\exp\left[\frac{E}{R\overline{T}^2}\left(T-\overline{T}\right)\right] \tag{25}$$

Therefore, the correction coefficient F for cross-sectional average reaction rate can be derived by Eq. (26).

$$\begin{aligned}F&=\frac{\overline{R(T)}}{R\left(\overline{T}\right)}\\&=\frac{\int_0^{R_{\text{reactor}}}A\exp\left(\frac{E}{R\overline{T}}\right)\exp\left[\frac{E}{R\overline{T}^2}\left(T-\overline{T}\right)\right]\cdot 2\pi r\mathrm{d}r\Big/\pi R_{\text{reactor}}^2}{A\exp\left(\frac{E}{R\overline{T}}\right)}\\&=\frac{R\overline{T}\left(1+\frac{a}{2}\right)}{Ea}\left\{\exp\left[\frac{Ea}{2R\overline{T}\left(1+\frac{a}{2}\right)}\right]-\exp\left[\frac{-Ea}{2R\overline{T}\left(1+\frac{a}{2}\right)}\right]\right\}\end{aligned} \tag{26}$$

where E is the activity energy for chemical reaction, and the values are shown in Table 3.

Table 3 Activity energy for different chemical reactions[32]

Reaction	MSR	MD	WSR
E/ J·mol^{-1}	102800	170000	87600

Fig. 13 compares temperature and methanol conversion efficiency calculated by 2-dimensional

and 1-dimensional model. From Fig. 13 (a), clearly, it can be seen that for different catalytic activities (σ=0.2, 0.4, 0.6, 0.8, 1.0), the cross-sectional average temperature variations along flow direction predicted by 1-dimenional model and 2-dimensional model are quite close. And as can be found in Fig. 13 (b) that, the deviation between methanol conversion efficiencies calculated by 1-dimensional and 2-dimensional model are relatively small, and the largest deviation is 0.21 %, and as for the maximum catalyst temperature, the largest discrepancy is below 0.5 % when the σ ranges from 0.2 to 1.0. Therefore, it can be concluded that 1-dimensional model is accurate enough to predict the thermal and chemical performance of SPTRR with different catalytic activities.

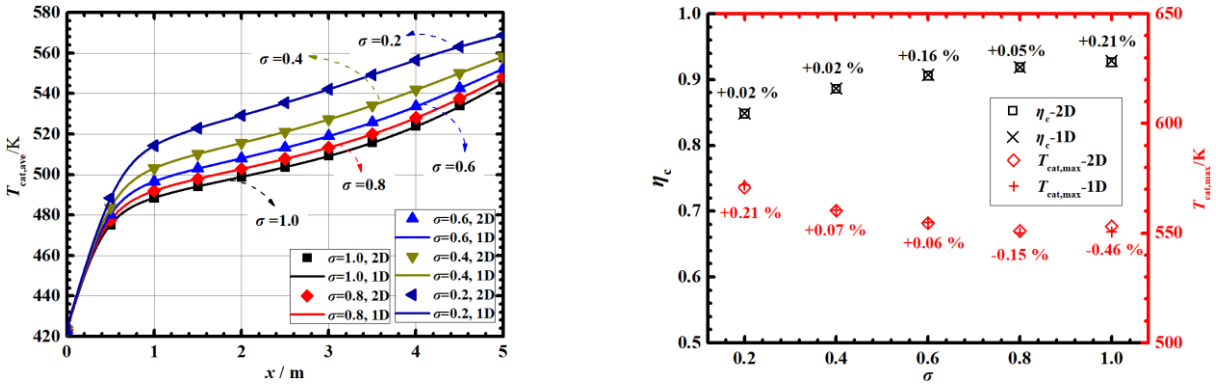

(a) Cross-sectional average temperature variation along flow direction

(b) Methanol conversion efficiency and max temperature of catalyst

Fig. 13 Comparison of results of temperature and methanol conversion efficiency calculated by two-dimensional and one-dimensional model

In addition, the comparison of computational cost between 1-dimensional and 2-dimensional model is performed on a computer with 8-core 2.3 GHz CPU and 32 GB RAM. For the case of SPTRR with catalytic activity of 0.8, the computing time of one-dimensional model is about 22 min for a steady condition case, which is much shorter than that of two-dimensional model (305 min). Therefore, it can be concluded that one-dimensional model is accurate enough and time-saving compared to two-dimensional model for simulating the heat transfer and chemical process of SPTRR，which is beneficial for quick performance prediction of SPTRR.

3.3.2 Distribution optimization of catalytic activity along axial direction

As mentioned above, the computing time of one-dimensional model for one case of SPTRR is

around 22 min, which is still relatively long to be applied for the optimization of catalytic activity distribution. To overcome this problem, BP (Back Propagation) neural network is adopted to predict the chemical performance of SPTRR with different catalytic activities, and one-dimensional model is employed to produce the training and validation data for the establishment and testing of BP neural network. The inputs of BP neural network are catalytic activities of each part (σ_1, σ_2 and σ_3), and output is methanol conversion efficiency. BP neural network is a multi-layer neural network, and has been widely applied in fields of image analysis and speech recognition due to its strong non-linear mapping ability, high self-learning and self-adaptive ability. Weights and thresholds during the signal transmission in BP neural network are key parameters for the accuracy of prediction, thus in present paper, genetic algorithm (GA) is used to optimize the training process of the neural network, and find optimal weights and thresholds that meet the requirements of the network. Table 4 lists the training and validation dataset for BP neural network, which contains 100 cases for neural net training, 32 cases for neural net validation and 16 cases for neural net testing.

Table 4 Training and validation dataset for BP neural network

Dataset	σ_1	σ_2	σ_3	Number of case
Training	0.2, 0.4, 0.8, 1.0	0, 0.2, 0.4, 0.6, 1.0	0, 0.2, 0.6, 0.8, 1.0	100
Validation	0.6	0.2, 0.4, 0.6, 1.0	0.2, 0.6, 0.8, 1.0	16
	0.2, 0.4, 0.8, 1.0	0.8	0.2, 0.6, 0.8, 1.0	16
Testing	0.2, 0.4, 0.8, 1.0	0.2, 0.4, 0.6, 1.0	0.4	16

Three-layer neural network is employed and the number of neurons in the hidden layer is set to 10. The trainlm function is used as training function, the upper number for training is 10000 and the convergence target is set to 1.0×10^{-7}. In genetic algorithm, the optimizing objective is shown in Eq. (27), and the parameters in optimization are listed in Table 5.

$$\min\left(\sqrt{\sum_{i=1}^{n}\left(\eta_{\mathrm{BP},i}-\eta_{\mathrm{validation},i}\right)^2}\right) \tag{27}$$

where $\eta_{\mathrm{BP},i}$ and $\eta_{\mathrm{validation},i}$ are methanol conversion efficiency predicted by BP neural network and from the validation dataset calculated by one-dimensional model, respectively, n is the number of case

in the validation dataset.

Table 5 Parameter in the optimizing process of genetic algorithm

Population size	Maximum generations	Binary digits of variable	Crossing probability	Mutation probability	Generation gap
100	100	10	0.7	0.01	0.95

Fig. 14 shows comparison of methanol conversion efficiency calculated by BP neural network and 2-D model. From this figure, it can be seen that the methanol conversion efficiency predicted by trained neural network matches well with the results calculated by 2-D model. Thus, the trained neural network can be used to predicting the methanol conversion efficiency of SPTRR with different catalytic activities.

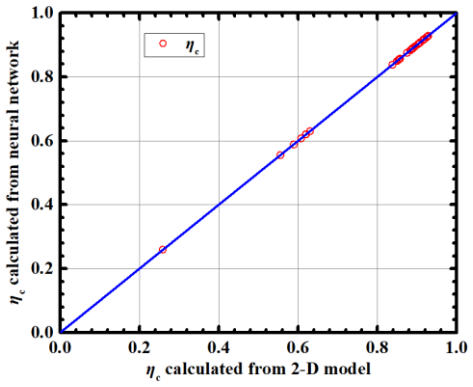

Fig. 14 Methanol conversion efficiency calculated from BP neural network and 2-D model

Furthermore, genetic algorithm is employed to optimize the distribution of catalytic activity along the flow direction based on the obtained BP neural network. In order to achieve efficient steady performance and stable dynamic behavior at the same time, i.e., high methanol conversion efficiency and low average catalytic activity, methanol conversion efficiency and average catalytic activity are combined as the optimization objective, which is defined as Eq. (28). To keep high methanol conversion efficiency and avoid the overshoot of catalyst temperature, the constraints on η_c and σ are considered, which are expressed as Eq. (29) and Eq. (30)

Optimization objective:

$$\mathrm{Max}\left(\eta_c \Big/ \left[\frac{(\sigma_1+\sigma_2+\sigma_3)}{3}\right]\right) \tag{28}$$

Constraints:

$$\eta_c > \eta_{c,0} \times 0.99 \tag{29}$$

$$0.2<\sigma_i<1,\ i=1,\ 2,\ 3 \tag{30}$$

where $\eta_{c,0}$ is the methanol conversion efficiency of SPTRR fully packed with catalyst.

The parameters of genetic algorithm for distribution optimization of catalytic activity are same with that for BP neural network, and the optimized distribution of catalytic activity by GA is listed in Table 6. As can be seen in this table, the optimized distribution of catalytic activity is σ_1=σ_1=0.2, σ_3=0.916 with the average catalytic activity of 0.44, and the predicted methanol conversion efficiency is 0.920.

Table 6 Optimal distribution of catalytic activity

σ_1	σ_2	σ_3	$\eta_{c,BP}$	$\eta_{c,2D}$	$\eta_{c,BP}\Big/\left[\frac{(\sigma_1+\sigma_2+\sigma_3)}{3}\right]$
0.2	0.2	0.916	0.920	0.919	2.097

Then, two-dimensional model is employed to calculate the methanol conversion efficiency of SPTRR with the optimal distribution of catalytic activity, and the calculated $\eta_{c,2D}$ is 0.919, which is relatively close to $\eta_{c,BP}$ (0.920) predicted by BP neural network, indicating that the predicted results by neural network are accurate and valid.

3.4 Steady and dynamic performance of SPTRR with optimal distribution of catalytic activity

After obtaining the optimal analytic activity distribution, in this section, the thermal and chemical performance of STRR filled with uniform and optimal distribution of analytic activity are compared and analyzed. In simulations, the results are calculated by 2-D model.

The maximum temperature of catalyst and methanol conversion efficiency of SPTRR with different catalytic activity distributions of $\sigma_{uniform}$=1, $\sigma_{uniform}$=0.44 and $\sigma_{optimal}$ are compared, which shown in Fig. 15 (a). It is found that for these three catalytic activity distributions, the highest temperatures of catalyst are all below the upper limit temperature of catalyst (573 K), which can ensure the safe and long-term run of SPTRR. Among these three catalytic activity distributions, SPTRR with $\sigma_{uniform}$=0.44 has the highest catalyst temperature of 560.9 K, then is SPTRR with

$\sigma_{uniform}$=1, and SPTRR with $\sigma_{optimal}$ has the lowest catalyst temperature of 549.5 K, indicating that SPTRR with $\sigma_{optimal}$ is farthest away from the catalyst limit temperature and can handle the sudden uprising of solar radiation best. For the chemical performance, although the average catalytic activity is 0.44, with 56 % less of catalyst, methanol conversion efficiency of SPTRR with $\sigma_{optimal}$ is similar with that of SPTRR fully packed with catalyst ($\sigma_{uniform}$=1), and larger than that of SPTRR with $\sigma_{uniform}$=0.44. It can be concluded that with much less catalyst and high content of EPCM, SPTRR with optimal distribution of catalytic activity can keep similar steady thermal and chemical performance with SPTRR with fully packed with catalyst.

Due to the low methanol conversion efficiency of SPTRR filled with $\sigma_{optimal=0.44}$ under steady condition of solar radiation, only dynamic behavior comparison of SPTRR with $\sigma_{uniform}$=1 and $\sigma_{optimal}$ under unsteady condition of solar radiation are compared, which is illustrated in Fig. 15 (b). Clearly, as can be seen from this figure, when SPTRR is under single step fluctuation of solar radiation, compared with $\sigma_{uniform}$=1, the delay response time $\Delta t_{50,\eta_c}$ of SPTRR with $\sigma_{optimal}$ is much prolonged from 1.3 mins to 2.8 mins, nearly improved by 115.4%. And when SPTRR is under the successive fluctuation of solar radiation, the relatively vibrating amplitude γ_{η_c} of SPTRR with $\sigma_{optimal}$ is largely alleviated from 0.78 to 0.32, which is almost reduced by 60 %, compared to that of SPTRR with $\sigma_{uniform}$=1. Therefore, it can be concluded that compared with $\sigma_{uniform}$=1, SPTRR with $\sigma_{optimal}$ has larger thermal inertia to leave more time for controller to take action and shows more stable dynamic behavior under the fluctuation of solar radiation.

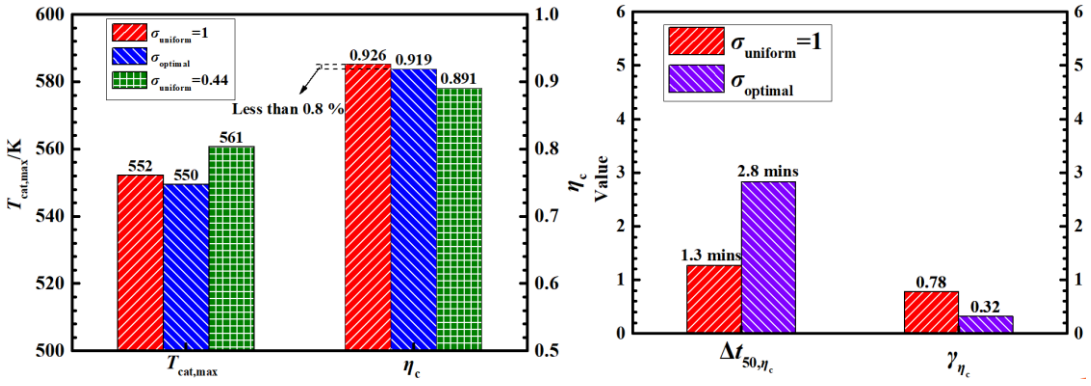

(a) Steady performance (b) Dynamic performance

Fig. 15 Steady and dynamic performance comparison of SPTRR with different distributions of catalytic activity

4. Conclusion

In this study, the catalytic activity of solar thermochemical reactor is adjusted by the diluting catalyst with EPCM to improve the steady and dynamic performance of SPTRR. At first, a two-dimensional model is established to compare steady performance of reactor with different catalytic activities. Then, one-dimensional model is derived from two-dimensional model and used to train BP neural network. Finally, optimal distribution of catalytic activity is obtained by genetic algorithm and BP neural network, and the steady and dynamic performance of SPTRR with uniform distribution and optimal distribution are compared. The salient findings are as follows:

(1) For steady performance of solar thermochemical reactor, when catalytic activity decreases from 1.0 to 0.2, the maximum temperature of catalyst increases from 552 to 573 K, which is still within the allowable temperature range of $Cu/ZnO/Al_2O_3$ catalyst for safe operation, and methanol conversion efficiency and $\dot{m}_{H_2}$ are reduced by 8.4 % and 9.9 % respectively, while $\dot{m}_{CO}$ rises by 121.3 %.

(2) For the dynamic performance, compared with solar thermochemical reactor fully packed with catalyst (σ=1), when σ is diluted by encapsulated phase change material to 0.4, $\Delta t_{50,\eta_c}$ of reactor under single-step fluctuation of solar radiation is prolonged by 845 % and relatively vibrating amplitude of methanol conversion efficiency is reduced by 69.8 %, which shows better stability.

(3) One-dimensional simplified model derived in present study is accurate enough and time-saving compared to two-dimensional model.

(4) With 56 % less of catalyst, solar thermochemical reactor with optimal distribution of catalytic activity can keep similar steady thermal and chemical performance with SPTRR fully packed with catalyst.

Acknowledgement

This research is supported by the National Natural Science Foundation of China (No. 51976156, 51906186).

The authors would also like to thank the Foundation for Innovative Research Groups of the National Natural Science Foundation of China (No.51721004) and the Foundation for San Qin Scholar Innovative Research Groups of Shaanxi Province.

Nomenclature and units

c_p	specific heat, $J \cdot kg^{-1} \cdot K^{-1}$
d_{cat}	diameter of catalyst particles, m
D	diameter, m
f_{EPCM}	volume ratio of EPCM to mixture
h_0	formation enthalpy, $J \cdot mol^{-1}$
k_{cat}	permeability of catalyst, m^2
k	turbulence kinetic energy, $m^2 \cdot s^{-2}$
L	latent heat, $J \cdot kg^{-1}$
L_{tube}	length of tube, m
$\dot{m}$	mass flow rate, $kg \cdot h^{-1}$
m_i	mass fraction of species i
M_i	mole fraction of species i
$M_{w,i}$	molecular weight of species i, $kg \cdot mol^{-1}$
n	molar flow rate, $mol \cdot s^{-1}$

$\hat{R}_{i,r}$	rates of creation and destruction of species *i* in the reaction *r*, $mol \cdot m^{-3} \cdot s^{-1}$
Sc_t	effective turbulent Schmidt number
t	time, s
T	temperature, K
p	pressure, Pa
Q	total heat transfer rate, W
R	universal gas constant, $J \cdot mol^{-1} \cdot K^{-1}$
R_R	reaction rate of methanol steam reforming reaction, $mol \cdot m^{-3} \cdot s^{-1}$
R_D	reaction rate of methanol decomposition reaction, $mol \cdot m^{-3} \cdot s^{-1}$
R_W	reaction rate of water shift reaction, $mol \cdot m^{-3} \cdot s^{-1}$
$\vec{u}$	velocity vector, $m \cdot s^{-1}$

Greek symbols

β	inertial loss coefficient, m^{-1}
γ_{η_c}	relatively vibrating amplitude of methanol conversion efficiency
$\Delta t_{50,\eta_c}$	delay response time of methanol conversion efficiency, s
δ_{ij}	Kronecker's delta
ε	turbulence kinetic energy dissipation rate, $m^2 \cdot s^{-3}$
ε_{mix}	porosity of packed mixture of catalyst and EPCM
η_c	methanol conversion efficiency
λ	thermal conductivity, $W \cdot m^{-1} \cdot K^{-1}$

μ	dynamic viscosity, Pa·s
μ_t	turbulent viscosity, Pa·s
ρ	density, kg·m^{-3}
σ	catalytic activity

Subscripts

ave	average
cat	catalyst
eff	effective
f	fluid
i	species
mix	mixture of catalyst and EPCM
s	solid

Abbreviations

DNI	direct normal irradiance
EPCM	Encapsulated phase change material
MD	methanol decomposition
MSR	methanol steam reforming
PCM	phase change material
SPTRR	solar parabolic trough receiver reactor

WSR water–gas shift reaction

References

[1] Li MJ, Tao WQ. Review of methodologies and polices for evaluation of energy efficiency in high energy-consuming industry. Applied Energy. 2017;187:203-15.

[2] Yadav D, Banerjee R. A review of solar thermochemical processes. Renewable & Sustainable Energy Reviews. 2016;54:497-532.

[3] Wang YJ, Liu QB, Sun J, Lei J, Ju Y, Jin HG. A new solar receiver/reactor structure for hydrogen production. Energy Conversion and Management. 2017;133:118-26.

[4] Liu XF, Hong H, Jin HG. Mid-temperature solar fuel process combining dual thermochemical reactions for effectively utilizing wider solar irradiance. Applied Energy. 2017;185:1031-9.

[5] Hao Y, Jin J, Jin HG. Thermodynamic analysis of isothermal CO2 splitting and CO2-H2O co-splitting for solar fuel production. Applied Thermal Engineering. 2019;166:113600.

[6] Chuayboon S, Abanades S, Rodat S. Syngas production via solar-driven chemical looping methane reforming from redox cycling of ceria porous foam in a volumetric solar reactor. Chemical Engineering Journal. 2019;356:756-70.

[7] Romero M, Steinfeld A. Concentrating solar thermal power and thermochemical fuels. Energy & Environmental Science. 2012;5:9234-45.

[8] Liu QB, Wang YJ, Lei J, Jin HG. Numerical investigation of the thermophysical characteristics of the mid-and-low temperature solar receiver/reactor for hydrogen production. International Journal of Heat and Mass Transfer. 2016;97:379-90.

[9] Jiang Q, Zhang H, Deng Yn, Kang Q, Hong H, Jin H. Properties and reactivity of LaCuxNi1−xO3 perovskites in chemical-looping combustion for mid-temperature solar-thermal energy storage. Applied energy. 2018;228:1506-14.

[10] Iulianelli A, Ribeirinha P, Mendes A, Basile A. Methanol steam reforming for hydrogen generation via conventional and membrane reactors: a review. Renewable and Sustainable Energy Reviews. 2014;29:355-68.

[11] Liu QB, Hong H, Yuan JL, Jin HG, Cai RX. Experimental investigation of hydrogen production integrated methanol steam reforming with middle-temperature solar thermal energy. Applied Energy. 2009;86:155-62.

[12] Rowe SC, Hischier I, Palumbo AW, Chubukov BA, Wallace MA, Viger R, et al. Nowcasting, predictive control, and feedback control for temperature regulation in a novel hybrid solar-electric reactor for continuous solar-thermal chemical processing. Solar Energy. 2018;174:474-88.

[13] Saade E, Clough DE, Weimer AW. Model predictive control of a solar-thermal reactor. Solar Energy. 2014;102:31-44.

[14] Petrasch J, Osch P, Steinfeld A. Dynamics and control of solar thermochemical reactors. Chemical Engineering Journal. 2009;145:362-70.

[15] Roca L, de la Calle A, Yebra LJ. Heliostat-field gain-scheduling control applied to a two-step

solar hydrogen production plant. Applied energy. 2013;103:298-305.
[16] Muroyama A, Shinn T, Fales R, Loutzenhiser PG. Modeling of a dynamically-controlled hybrid solar/autothermal steam gasification reactor. Energy & Fuels. 2014;28:6520-30.
[17] Kuhn P, Wilbert S, Schüler D, Prahl C, Haase T, Ramirez L, et al. Validation of spatially resolved all sky imager derived DNI nowcasts. AIP conference proceedings: AIP Publishing; 2017. p. 140014.
[18] Odunsi AO, O'Donovan TS, Reay DA. Temperature stabilisation in Fischer-Tropsch reactors using phase change material (PCM). Applied Thermal Engineering. 2016;93:1377-93.
[19] Jiang G, Huang J, Liu M, Cao M. Experiment and simulation of thermal management for a tube-shell Li-ion battery pack with composite phase change material. Applied Thermal Engineering. 2017;120:1-9.
[20] Ma Z, Yang WW, Yuan F, Jin B, He YL. Investigation on the thermal performance of a high-temperature latent heat storage system. Applied Thermal Engineering. 2017;122:579-92.
[21] Huang YH, Cheng WL, Zhao R. Thermal management of Li-ion battery pack with the application of flexible form-stable composite phase change materials. Energy Conversion and Management. 2019;182:9-20.
[22] Pattison RC, Baldea M. A thermal ‐ flywheel approach to distributed temperature control in microchannel reactors. AIChE journal. 2013;59:2051-61.
[23] Hatamachi T, Kodama T, Isobe Y, Nakano D, Gokon N. Double-walled reactor tube with molten salt thermal storage for solar tubular reformers. Journal of Solar Energy Engineering-Transactions of the Asme. 2006;128:134-8.
[24] Gokon N, Nakano D, Inuta S, Kodama T. High-temperature carbonate/MgO composite materials as thermal storage media for double-walled solar reformer tubes. Solar Energy. 2008;82:1145-53.
[25] Zhang M, Hong Y, Ding S, Hu J, Fan Y, Voevodin AA, et al. Encapsulated nano-heat-sinks for thermal management of heterogeneous chemical reactions. Nanoscale. 2010;2:2790.
[26] Li MJ, Jin B, Ma Z, Yuan F. Experimental and numerical study on the performance of a new high-temperature packed-bed thermal energy storage system with macroencapsulation of molten salt phase change material. Applied Energy. 2018;221:1-15.
[27] Odunsi AO, O'Donovan TS, Reay DA. Dynamic Modeling of Fixed ‐ Bed Fischer ‐ Tropsch Reactors with Phase Change Material Diluents. Chemical Engineering & Technology. 2016;39:2066-76.
[28] Calverley EM, Witt PM, Sweeney JD. Reactor runaway due to statistically driven axial activity variations in graded catalyst beds. Chemical engineering science. 2012;80:393-401.
[29] Melis S, Varma A, Pereira CJ. Optimal distribution of catalyst for a case involving heterogeneous and homogeneous reactions. Chemical engineering science. 1997;52:165-9.
[30] Nie Y, Witt PM, Agarwal A, Biegler LT. Optimal active catalyst and inert distribution in catalytic packed bed reactors: ortho-xylene oxidation. Industrial & Engineering Chemistry Research. 2013;52:15311-20.
[31] Zheng ZJ, He Y, He YL, Wang K. Numerical optimization of catalyst configurations in a solar parabolic trough receiver-reactor with non-uniform heat flux. Solar Energy. 2015;122:113-25.
[32] Peppley BA, Amphlett JC, Kearns LM, Mann RF. Methanol–steam reforming on Cu/ZnO/Al 2 O 3 catalysts. Part 2. A comprehensive kinetic model. Applied Catalysis A General.

1999;179:31-49.
[33] Zheng ZJ, He Y, He YL, Wang K. Numerical optimization of catalyst configurations in a solar parabolic trough receiver–reactor with non-uniform heat flux. Solar Energy. 2015;122:113-25.
[34] Wang YJ, Liu QB, Lei J, Jin HG. A three-dimensional simulation of a parabolic trough solar collector system using molten salt as heat transfer fluid. Applied Thermal Engineering. 2014;70:462-76.
[35] He YL, Wang K, Qiu Y, Du BC, Liang Q, Du S. Review of the solar flux distribution in concentrated solar power: non-uniform features, challenges, and solutions. Applied Thermal Engineering. 2018;230:448-74.
[36] Gee R, Winston R. A Non-Imaging Secondary Reflector for Parabolic Trough Concentrators. Report to NREL, Duke Solar Energy, Raleigh, NC. 2001.
[37] Tsai CY, Lin PD. Optimized variable-focus-parabolic-trough reflector for solar thermal concentrator system. Solar Energy. 2012;86:1164-72.
[38] Wang K, He YL, Li P, Li MJ, Tao WQ. Multi-objective optimization of the solar absorptivity distribution inside a cavity solar receiver for solar power towers. Solar Energy. 2017;158:247-58.
[39] Qiu Y, He YL, Li PW, Du BC. A comprehensive model for analysis of real-time optical performance of a solar power tower with a multi-tube cavity receiver. Applied energy. 2017;185:589-603.
[40] Hsueh CY, Chu HS, Yan WM, Leu GC, Tsai JI. Three-dimensional analysis of a plate methanol steam micro-reformer and a methanol catalytic combustor with different flow channel designs. International Journal of Hydrogen Energy. 2011;36:13575-86.
[41] Ma Z, Yang WW, Li MJ, He YL. High efficient solar parabolic trough receiver reactors combined with phase change material for thermochemical reactions. Applied energy. 2018;230:769-83.
[42] Fridman E. Introduction to time-delay systems: Analysis and control: Springer; 2014.
[43] Tao WQ. Numerical heat transfer: Xi'an Jiaotong University Press, Xi'an; 2001.
[44] Sinnott RK. Chemical engineering design: Elsevier; 2014.